JOURNAL OF THE AMERICAN WATER RESOURCES ASSOCIATION
Vol. 52, No. 1 AMERICAN WATER RESOURCES ASSOCIATION February 2016

BENCHMARKING OPTICAL/THERMAL SATELLITE IMAGERY FOR ESTIMATING EVAPOTRANSPIRATION AND SOIL MOISTURE IN DECISION SUPPORT TOOLS[1]

Jan M.H. Hendrickx, Richard G. Allen, Al Brower, Aaron R. Byrd, Sung-ho Hong, Fred L. Ogden, Nawa Raj Pradhan, Clarence W. Robison, David Toll, Ricardo Trezza, Todd G. Umstot, and John L. Wilson[2]

ABSTRACT: Generally, one expects evapotranspiration (ET) maps derived from optical/thermal Landsat and MODIS satellite imagery to improve decision support tools and lead to superior decisions regarding water resources management. However, there is lack of supportive evidence to accept or reject this expectation. We "benchmark" three existing hydrologic decision support tools with the following benchmarks: annual ET for the ET Toolbox developed by the United States Bureau of Reclamation, predicted rainfall-runoff hydrographs for the Gridded Surface/Subsurface Hydrologic Analysis model developed by the U.S. Army Corps of Engineers, and the average annual groundwater recharge for the Distributed Parameter Watershed Model used by Daniel B. Stephens & Associates. The conclusion of this benchmark study is that the use of NASA/USGS optical/thermal satellite imagery can considerably improve hydrologic decision support tools compared to their traditional implementations. The benefits of improved decision making, resulting from more accurate results of hydrologic support systems using optical/thermal satellite imagery, should substantially exceed the costs for acquiring such imagery and implementing the remote sensing algorithms. In fact, the value of reduced error in estimating average annual groundwater recharge in the San Gabriel Mountains, California alone, in terms of value of water, may be as large as $1 billion, more than sufficient to pay for one new Landsat satellite.

(KEY TERMS: soil moisture; evapotranspiration; GSSHA; SEBAL; METRIC; DPWM; distributed hydrologic modeling; optical/thermal satellite imagery; Landsat; MODIS; groundwater recharge; water management; hydrograph.)

Hendrickx, Jan M.H., Richard G. Allen, Al Brower, Aaron R. Byrd, Sung-ho Hong, Fred L. Ogden, Nawa Raj Pradhan, Clarence W. Robison, David Toll, Ricardo Trezza, Todd G. Umstot, and John L. Wilson, 2016. Benchmarking Optical/Thermal Satellite Imagery for Estimating Evapotranspiration and Soil Moisture in Decision Support Tools. *Journal of the American Water Resources Association* (JAWRA) 52(1): 89-119. DOI: 10.1111/1752-1688.12371

[1]Paper No. JAWRA-14-0179-P of the *Journal of the American Water Resources Association* (JAWRA). Received August 27, 2014; accepted September 28, 2015. **Discussions are open until six months from issue publication**.

[2]Professor (Hendrickx, Wilson), Department of Earth and Environmental Sciences, New Mexico Tech, 801 Leroy Place, Socorro, New Mexico 87801; Professor (Allen), Research Associate (Robison), Associate Research Professor (Trezza), Kimberly Research and Extension Center, University of Idaho, Kimberly, Idaho 83341; Retired Civil Engineer (Brower), Water and Environmental Resources Division, U.S. Bureau of Reclamation, Denver, Colorado 80225; Hydraulics Research Civil Engineer (Byrd, Pradhan), Engineer Research and Development Center, U.S. Army Corps of Engineers, Vicksburg, Mississippi 39180; Assistant Professor (Hong), Department of Geosciences, Murray State University, Murray, Kentucky 42071; Professor (Ogden), Water Resources/Environmental Science and Engineering, University of Wyoming, Laramie, Wyoming 82071; Retired Deputy Program Manager (Toll), Hydrological Sciences Lab, NASA Goddard Space Flight Center, Greenbelt, Maryland 20771; and Senior Hydrogeologist (Umstot), Daniel B. Stephens and Associates, Inc., Albuquerque, New Mexico 87109 (E-Mail/Hendrickx: hendrick@nmt.edu).

INTRODUCTION

Monitoring of regional evapotranspiration (ET) allows decision makers to (1) follow where, when, and how much water has moved into the atmosphere by ET; (2) monitor crop performance and the effects of drought for famine prediction; (3) better evaluate the performance of irrigation systems; (4) improve estimates by distributed hydrologic and weather models; and (5) estimate root zone soil moisture conditions. It is expected that the integration of regional ET maps derived from National Aeronautics and Space Administration (NASA) and United States Geological Survey (USGS) earth imaging products will improve decision support tools and, therefore, lead to superior decisions regarding water resources utilization. However, there is a need to quantify benefits realized through the use of satellite derived results in user decision support tools. When our study started in 2006, only a few research examples had been reported in the literature where NASA earth science results related to ET had been integrated into hydrologic models (Ahmad and Bastiaanssen, 2003; Schuurmans *et al.*, 2003) but no operational hydrologic decision support tools were known to our research team that used satellite-estimated ET products on a regular basis.

Therefore, the overall goal of this study was to see if the use of satellite optical/thermal imagery improves the performance of three operational hydrologic decision support tools: the ET Toolbox developed by the United States Bureau of Reclamation (USBR), the Gridded Surface/Subsurface Hydrologic Analysis (GSSHA) model developed by the U.S. Army Corps of Engineers, and the Distributed Parameter Watershed Model (DPWM) based on the Mass Accounting System for Soil Infiltration and Flow (MASSIF) model, developed in 2007 by Sandia National Laboratory, and since then continuously improved by Daniel B. Stephens & Associates (DBS&A) for the prediction of groundwater recharge in semiarid regions.

The ET Toolbox is a grid-based approach that uses the "crop coefficient reference ET approach" (Allen *et al.*, 1998; Jensen, 1998) to provide daily forecasts of water depletions, i.e., ET of agricultural and riparian vegetation as well as evaporation from open water, for the day in question and the following six days (Brower, 2008). The GSSHA (Downer and Ogden, 2004, 2006) is a physically based, distributed hydrologic model that simulates the hydrologic response of a watershed subject to given hydrometeorological inputs. It is used by the U.S. Army Corps of Engineers not only within the United States (U.S.) but also worldwide. The DPWM (Daniel B. Stephens & Associates, Inc., 2010a) is a distributed hydrologic model used for the evaluation of groundwater recharge in arid and semiarid basins (e.g., Daniel B. Stephens & Associates, Inc., 2008, 2010b, 2011; Hendrickx *et al.*, 2011a).

In the context of this study, benchmarking is the process of running a hydrologic decision support tool to assess the relative performance of using optical/thermal satellite imagery for the improvement of forcing functions (e.g., precipitation, ET, etc.), the appraisal of initial conditions (e.g., soil moisture, snow cover, etc.), and the estimation of model parameters (e.g., land use, soil texture, total available water for transpiration) (Toll, 2008). Our study objective was to benchmark traditional applications of ET Toolbox, GSSHA, and DPWM versus the use of optical/thermal satellite imagery on the forcing function of ET in ET Toolbox, the appraisal of initial soil moisture conditions in GSSHA, and the estimation of the model parameter "total available water for transpiration (TAW)" in DPWM.

BENCHMARKING METHOD

Our benchmarking method compared typical traditional applications of each decision support tool with ones that used information from optical/thermal satellite imagery. The comparisons were based on a "performance indicator," i.e., a measurement for assessing the quantitative performance of a system. The performance indicators selected were: annual ET forecasts for ET Toolbox, storm hydrographs for GSSHA, and average annual groundwater recharge volumes for DPWM. The goal of our research sponsor NASA was to benchmark the improvement, if any, to the "performance indicators" from the use of satellite imagery for the purpose of improving decision making in water resources management.

First, the optical/thermal satellite images were converted into maps of ET and root zone soil moisture with established algorithms: *Surface Energy Balance Algorithms for Land (SEBAL)*, *Mapping EvapoTranspiration (ET) at high Resolution with Internalized Calibration (METRIC)*, and the *Evaporative Fraction Method for Root Zone Soil Moisture Retrieval*. The inputs for these algorithms are the bands of Landsat and the Moderate Resolution Imaging Spectroradiometer (MODIS) presented in Table 1. The ET maps were then incorporated into the hydrologic decision support tools, either after conversion of the ET into the reference ET fraction (ETrF) using high-quality hourly weather data, or — where this was

TABLE 1. Band Spatial Resolutions (m) and Wavelengths (μm) of Landsat 5 and 7 and MODIS Sensors.

Sensors		Band number								
		1	2	3	4	5[1]	6	7	31	32
Landsat7 Landsat5	Pixel size (m)	30	30	30	30	30	60 (L7) 120 (L5)	30	NA[2]	NA[2]
	Band width (μm)	0.45-0.51	0.52-0.60	0.63-0.69	0.75-0.9	1.55-1.75	10.4-12.5	2.09-2.35	NA[2]	NA
MODIS	Pixel size (m)	250	250	500	500	500	500	500	1,000	1,000
	Band width (μm)	0.62-0.67	0.84-0.87	0.46-0.48	0.54-0.56	1.23-1.25	1.63-1.65	2.11-2.15	10.8-11.3	11.8-12.3

[1]MODIS band 5 is not used in this study because of streaking noise.
[2]Not available.

not possible — after conversion of the heat fluxes retrieved with SEBAL or METRIC into root zone soil moisture. The details of these three operations are presented below.

The SEBAL/METRIC Approach

SEBAL (Bastiaanssen *et al.*, 1998a, 2005) and METRIC (Allen *et al.*, 2007a, b) are "snapshot" energy balance models that use the strong thermal signals sensed by satellites that are associated with evaporation processes to provide high-resolution ET images. Spatial resolutions of retrievals range from 30 to 120 m with Landsat satellite data (Allen *et al.*, 2007a, 2011) and 250 to 1,000 m with MODIS (Allen *et al.*, 2008b; Trezza *et al.*, 2013). These energy balance algorithms are thermally driven, with ET computed as a residual of the surface energy balance, so that air humidity, air temperature, and vegetation canopy conductivities are not needed at each pixel of the image. METRIC employs an innovative Calibration using Inverse Modeling at Extreme Conditions method (Allen *et al.*, 2011; Irmak *et al.*, 2011; Irmak *et al.*, 2012) pioneered in the SEBAL model (Bastiaanssen *et al.*, 1998a) to overcome biases in land surface temperature retrievals and unknown spatial variation in near-surface air temperature during the estimation of sensible heat flux. As this calibration is based on a "cold" and "hot" pixel selected from within the image, it is often called an "internal" calibration. The METRIC/SEBAL approach has demonstrated ET accuracies of 15, 10, and 5% for daily, monthly, and seasonal time scales, respectively (Allen, 1997; Hendrickx and Hong, 2005; Allen *et al.*, 2007b; Hong, 2008). In this study, METRIC was used to benchmark the ET Toolbox and DPWM, while SEBAL was used for GSSHA. The main practical difference between METRIC and SEBAL is that the latter can be implemented without using meteorological observations—with some unknown decrease in accuracy—while METRIC needs hourly meteorological measurements including air humidity and temperature, wind speed, and solar radiation for calculation of the reference ET at one or more sites that are representative of the entire image or part of the image (Allen *et al.*, 2007a). The METRIC algorithm takes into account the effects of slope, aspect, and elevation on the energy balance which is critical for its application in mountains and over rolling terrain. It also captures the changes in soil evaporation and riparian vegetation transpiration due to capillary fluxes originating from the interaction between groundwater depth, soil texture, and even groundwater salinity. METRIC/SEBAL has been successfully used with Landsat and MODIS images in numerous practical applications (Bastiaanssen, 2000; Bastiaanssen *et al.*, 2000, 2002; Hafeez *et al.*, 2006; Allen *et al.*, 2008b; Hong *et al.*, 2009, 2011b). The ET estimates have, in turn, been used to derive evaporative fraction and soil moisture retrievals.

Like SEBAL, METRIC computes the latent heat flux as the residual of the surface energy balance

$$\lambda E = R_n - G - H \quad (1)$$

where R_n is net radiation, G the soil heat flux, H the sensible heat flux, and λE is the latent heat flux. METRIC deviates from SEBAL in its use of an internal calibration of the energy balance that incorporates effects of regional advection of energy and dry air, via the employment of the Penman-Monteith equation, that can substantially increase ET from irrigated agriculture and riparian vegetation (Allen *et al.*, 2007a) in semiarid and arid climates. METRIC retrievals of ET, when derived from Landsat or MODIS imagery, represent snapshots of ET during late morning. These time-snapshots are extended to daily totals using the fraction of reference ET, ETrF, a concept applied in METRIC, as the ETrF has been shown to be nearly constant over the course of a day for normal agricultural conditions (Allen *et al.*, 2007a, b). However, evaporative fraction has been suggested in place of ETrF for substantially stressed

conditions such as exist for natural conditions (Allen *et al.,* 2011) following Brutsaert and Sugita (1992) and Bastiaanssen *et al.* (1998a). They also suggest using evaporative fraction for regional, rainfed conditions where, by definition, advection is small or nonexistent.

The Evaporative Fraction Method for Soil Moisture Retrieval in the Root Zone

This method is based on the long-known soil physical relationship between root zone soil moisture and the partitioning of sensible and latent heat fluxes at the land surface (Davies and Allen, 1973; De Bruin, 1983; Owe and van de Griend, 1990; Kustas and Norman, 1999). This method is a straightforward extension of the METRIC and SEBAL algorithms that derives reliable estimates of the energy balance fluxes from remotely sensed optical/thermal imagery (Bastiaanssen *et al.*, 1997, 1998a, b, 2005; Ahmad and Bastiaanssen, 2003; Scott *et al.*, 2003; Fleming *et al.*, 2005; Hendrickx and Hong, 2005; Hong *et al.*, 2005).

In many agro-hydrologic studies, root zone soil moisture is used to reduce potential ET to actual ET (Feddes *et al.*, 1978, 1988; Belmans *et al.*, 1983; Wagenet and Hutson, 1996; Allen, 2000; Anderson *et al.*, 2007; Hain *et al.*, 2009, 2011). When soil moisture in the root zone decreases and soil resistance to water movement increases, the net effect is a reduction in actual ET (λE). When the soil is wet, most of the available energy (net radiation, R_n, minus soil heat flux, G) is used for ET (latent heat flux) and almost no energy is left for sensible heat flux (H). When the soil is dry, most of the available energy is used to heat soil and air and latent heat flux (ET) is small. One way to express this partitioning of radiant energy is the evaporative fraction (Λ) that is defined as (Brutsaert and Sugita, 1992; Crago, 1996):

$$\Lambda = \frac{\lambda E}{\lambda E + H} = \frac{\lambda E}{R_n - G} \tag{2}$$

The energy partitioning calculated with the evaporative fraction is primarily related to the amount of vegetation and soil moisture content (Boni *et al.*, 2001). The following equation was derived by Ahmad and Bastiaanssen (2003) using *in situ* root zone soil moisture measurements and validated evaporative fraction data from the SEBAL

$$S = \frac{\theta}{\theta_{sat}} = e^{\frac{\Delta - 1}{0.42}} \tag{3}$$

where S is degree of saturation (0.0-1.0), θ is volumetric water content, and θ_{sat} is volumetric water content at saturation. Equation (3) was derived from soil moisture measurements obtained on grassland in Kansas on alluvial soils and loess (Smith *et al.*, 1992), as well as from rainfed (vineyard, barley, wheat) and irrigated crops (maize, alfalfa) in Central Spain on sandy loams (Bolle *et al.*, 1993; Bastiaanssen *et al.*, 1997). A number of studies have successfully supported the use of Equation (3) for retrieval of root zone soil moisture using remote sensing algorithms (Scott *et al.*, 2003; Mohamed *et al.*, 2004; Fleming *et al.*, 2005).

Insertion of ET Fluxes in Hydrologic Models

The SEBAL/METRIC algorithms for ET mapping cannot provide a continuous series of daily ET estimates due to the fact that Landsat and MODIS images are only periodically available. Landsat imagery is potentially available every 16 days per satellite, while the daily MODIS images can only be used every 4 to 5 days when the satellite has a viewing angle of less than about 15° to the area of interest (Trezza *et al.*, 2013). The nadir-angled images are needed for reliable ET estimates from SEBAL and METRIC (Allen *et al.*, 2008b). In addition, the presence of clouds often causes longer time periods between images.

Another issue with constructing continuous series of ET with satellite imagery is the large temporal variability of ET fluxes. The daily ET can vary by a factor 2 or 3 from one day to another depending on weather conditions, especially cloudiness. As the ET observed from space on image days is often not representative of ET values on nonimage days, direct insertion of ET fluxes into hydrologic models can cause substantial error. Instead, more robust variables with less temporal variability such as the ETrF or *root zone soil moisture* (S or θ) are preferred for insertion into hydrologic decision support tools and for time-integration of ET between satellite overpass dates. As a consequence, the generation of a continuous series of daily ET maps is only possible by combining the available ET maps with a daily hydrologic model or other time-integration system that is based on relative ET, and for the same area or region.

The ETrF is calculated for each pixel of an image as

$$ET_rF = \frac{ET}{ET_r} \tag{4}$$

where ET is the actual ET estimated by SEBAL or METRIC for each pixel, and ET_r is the standardized reference ET for a tall crop (Allen *et al.*, 2005d). The ETrF is similar to the *crop coefficient* (K_c) that is defined as

$$K_c = \frac{ET_c}{ET_{ref}} \quad (5)$$

where ET_c is the crop ET under standard conditions and ET_{ref} is the (generic) reference ET. Crop ET under standard conditions refers to the actual ET from crops "that are grown in large fields under optimum soil water, excellent management condition and environmental conditions, and achieve full production under the given climatic conditions" (Allen *et al.*, 1998). The reference ET can be calculated for two types of reference surfaces representing clipped grass (a short, smooth crop) and alfalfa (a taller, rougher agricultural crop) resulting in, respectively, the reference ET for a short crop ET_o and for a tall crop ET_r (Allen *et al.*, 1998, 2005d). Due to the higher surface roughness of the tall crop, ET_r generally will be higher than ET_o for the same meteorological conditions (Irmak *et al.*, 2008). Therefore, one should use grass-based crop coefficients with ET_o and alfalfa-based crop coefficients with ET_r (Allen *et al.*, 2005d). If a reference ET other than ET_o or ET_r was used to develop the crop coefficients, it must be established that the equation yields values that are equivalent to ET_o or ET_r. For example, the daily "reference" ET that has been computed in the past by the New Mexico State University Penman equation ($ET_{o\text{-}NMSU}$) needs its own set of crop coefficients ($K_{c\text{-}NMSU}$) as explained in Case Study I.

Despite the similarity of Equations (4) and (5), a distinct difference can exist between reference ET fractions (ETrF) and traditional crop coefficients (K_c). The latter represent optimum agricultural management under well-watered conditions and are typically determined from point-based measurements; the former represent actual ETrF populations that may have inherent variation because of variation in water availability, crop variety, irrigation method, weather, soil type, salinity and fertility, and/or field management that can be different from the average K_c value for optimal crops.

The temporal robustness of the ETrF and K_c approach has been illustrated by lysimeter measurements for sugar beets that show ETrF and K_c values for sugar beets to be nearly identical on alternating clear and cloudy days with different ET values (Allen *et al.*, 2007b). Other agricultural crops, which are bred to maintain nearly constant and maximum stomatal conductivity so as to maximize biomass production, are expected to respond similarly. Thus, the daily ET for each pixel on nonimage days can be calculated using the ETrF derived by METRIC on the image day multiplied by the ET_r calculated from weather data on nonimage days. If two or more images are available, it is standard procedure to interpolate the ETrF between the image dates so that the dynamics of vegetation development are captured (Allen *et al.*, 2007a, 2011).

Root zone soil moisture is another robust hydrologic variable that is correlated with daily ET but without its large temporal variability (Hillel, 1998). For example, the dynamics of root zone soil moisture and actual ET at the Paynes Prairie State site in Florida show root zone soil moisture to vary gradually during the season, while the actual ET shows large variability from day to day caused by different weather conditions leading to different atmospheric demands (Jacobs *et al.*, 2002; Liu *et al.*, 2005).

Root zone soil moisture is an important tool for the incorporation of variable ET fluxes into hydrologic models when no high-quality hourly weather data are available to calculate ET_r during satellite overpass or in mountainous terrain where it is nearly impossible to estimate ET_r for each pixel due to the effects of slope, aspect, and elevation on incoming solar radiation, wind speed, air temperature, and relative humidity. Equations (2) and (3) show that the instantaneous heat fluxes from the METRIC/SEBAL approach yield sufficient information to obtain the root zone soil moisture condition of each pixel and to map soil moisture maps on image days for initialization of hydrologic models. For example, in GSSHA the actual ET, the potential evapotranspiration (PET), and volumetric soil water content are related as follows (Downer and Ogden, 2006):

$$ET = PET\left(\frac{\theta - \theta_{wp}}{0.75(\theta_{sat} - \theta_{wp})}\right) \quad (6)$$

where θ is the volumetric soil water content, θ_{wp} is the wilting point, and θ_{sat} is the saturated volumetric soil water content. If $\theta > 0.75\theta_{sat}$, the ET is considered equal to the PET. PET is considered equal to the reference ET for a tall crop (ET_r) that is calculated from the meteorological data measured at a ground-based station (Allen, 2001). The wilting point and the saturated volumetric water content are derived from the Natural Resource Conservation Service STATSGO database (*accessed* May 28, 2012, http://soildatamart.nrcs.usda.gov/) using established pedotransfer functions that yield θ_{wp} and θ_{sat} as a function of soil texture (Rawls *et al.,* 1982). Once GSSHA is initialized with a realistic soil moisture map, its daily ET predictions based on Equation (6) are expected to be more realistic as well. For long-term simulations, the soil moisture distribution of the model can be updated when new clear sky optical/thermal imagery becomes available.

CASE STUDY I: ET TOOLBOX IN THE MIDDLE RIO GRANDE CONSERVANCY DISTRICT

The ET Toolbox case study in the Middle Rio Grande Conservancy District (MRGCD) in New Mexico provides an example of how optical/thermal imagery can be used to derive the forcing function of ET in hydrologic models. The primary purpose of the ET Toolbox is to estimate daily water depletions, i.e., ET of agricultural and riparian vegetation as well as evaporation from open water, at a resolution of 1×1 km (previously 4×4 km), and to improve the efficiency of water management and irrigation scheduling by providing guidance — through ET charts — on when and where to deliver water and how much to apply (Brower, 2008). Daily ET forecasts for the day of interest and the following six days are accessible for water managers and other users through the internet (*accessed* August 30, 2011, www.usbr.gov/pmts/rivers/awards/Nm2/riogrande.html). For example, the Albuquerque office of the United States Bureau of Reclamation decides on a daily basis how much water to release from Cochiti reservoir to meet all agricultural, riparian, domestic, industrial, and minimum flow demands in the Rio Grande Valley between Cochiti and Elephant Butte reservoirs. As the travel time of river water from Cochiti reservoir to Elephant Butte reservoir is about five days (Langman, 2009), it is essential that the Bureau bases its releases on reliable ET forecasts. This information is critical because an error in the forecast "ends up in the river." If the ET forecast is larger than the actual ET, additional excess water may not be put to a beneficial use to those who could take the stored water later. On the other hand, if the forecast is smaller than the real ET, the legally binding minimum flow requirement of the river may be violated. This is especially important during periods of low flow and hot weather when a relatively small error in ET forecast can represent a considerable percentage of the minimum flow requirement.

The performance indicator used in evaluating the worth of ET estimates derived from NASA imagery on the ET Toolbox is the sum of all daily ET forecasts in 2007, i.e., the annual ET forecast. The inclusion of the ET forecasts for the following six days was also explored, but as they are usually similar to the first day's forecast under the climatic conditions of the MRGCD, only the first day's forecast was used. For this METRIC application we used MODIS imagery as its daily acquisition schedule all but assures that under the climatic conditions of MRGCD sufficient images will be available to force operational hydrologic decision support tools.

Benchmark Approach for ET Toolbox

We compared the annual sum of daily ET forecasts in 2007 using the traditional ET Toolbox approach ($ET_{Kc\text{-}NMSU}$) versus the annual sum derived from METRIC using 26 MODIS images distributed over the entire year (Table 2). The METRIC application resulted in twenty-six 500×500 m ETrF images that were aggregated to $1{,}000 \times 1{,}000$ m to coincide with the $1{,}000 \times 1{,}000$ m cell size of ET Toolbox. The 500×500 m pixels were developed by resampling 1,000 m MODIS thermal pixels to the 500 m resolution of most MODIS optical pixels (Trezza *et al.*, 2013). This was done to promote improved spatial fidelity of the ET retrievals. Following the production of ET, the product was resampled to the 1,000 m spatial resolution of the original thermal pixels. Figure 1 presents 12 monthly METRIC ETrF maps aggregated to 4×4 km to show the annual temporal and spatial dynamics of ETrF in the MRGCD. These METRIC ETrF values were used in two ways to estimate the annual sum of daily ET values: (1) the ETrF values were converted to ET Toolbox crop coefficients ($K_{c\text{-}METRIC}$) and then processed using the traditional ET Toolbox approach ($ET_{Kc\text{-}METRIC}$); (2) the ETrF values were processed using standard METRIC procedures without making use of ET Toolbox (ET_{METRIC}).

Traditionally, ET Toolbox has used the New Mexico State University Penman reference ET ($ET_{o\text{-}NMSU}$) instead of the ASCE Standardized Penman-Monteith reference ET (Brower, 2008) to calculate the crop ET under standard conditions as

$$ET_c = K_{c-NMSU} \times ET_{o-NMSU} \quad (7)$$

However the $ET_{o\text{-}NMSU}$, even though it is purported to be a grass reference method, produces higher

TABLE 2. Image Dates Used for the MODIS-METRIC Application in the Middle Rio Grande Valley of New Mexico for the Year 2007 (Allen *et al.*, 2008a).

Image No.	Date	Image No.	Date
1	January 28, 2007	14	June 30, 2007
2	February 6, 2007	15	July 7, 2007
3	January 1, 2007	16	July 16, 2007
4	March 17, 2007	17	August 8, 2007
5	March 26, 2007	18	August 24, 2007
6	April 2, 2007	19	September 18, 2007
7	April 18, 2007	20	September 25, 2007
8	April 27, 2007	21	October 11, 2007
9	May 13, 2007	22	October 20, 2007
10	May 29, 2007	23	October 27, 2007
11	June 5, 2007	24	November 21, 2007
12	June 14, 2007	25	December 23, 2007
13	June 21, 2007	26	December 30, 2007

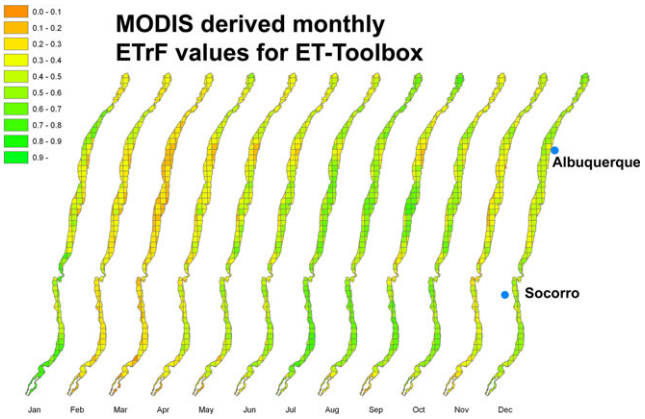

FIGURE 1. Monthly ETrF Aggregated to 4 km Sized Grid Cells of the ET Toolbox Grid along the Middle Rio Grande during 2007 (Allen *et al.*, 2008b).

estimates than the standard grass-reference ET_o of ASCE and FAO (Allen *et al.*, 2008a), and even exceeds the standardized ASCE alfalfa reference ET_r by 7.7% (Figure 2). Therefore, that reference method requires its own set of crop coefficients ($K_{c\text{-}NMSU}$) that were provided by Dr. Salim Bawazir of New Mexico State University on March 16, 2000 (Brower, 2008). In 2012, the ET Toolbox abandoned the New Mexico State University reference ET and switched to the ASCE Standardized Penman-Monteith reference ET method of Allen *et al.* (2005d).

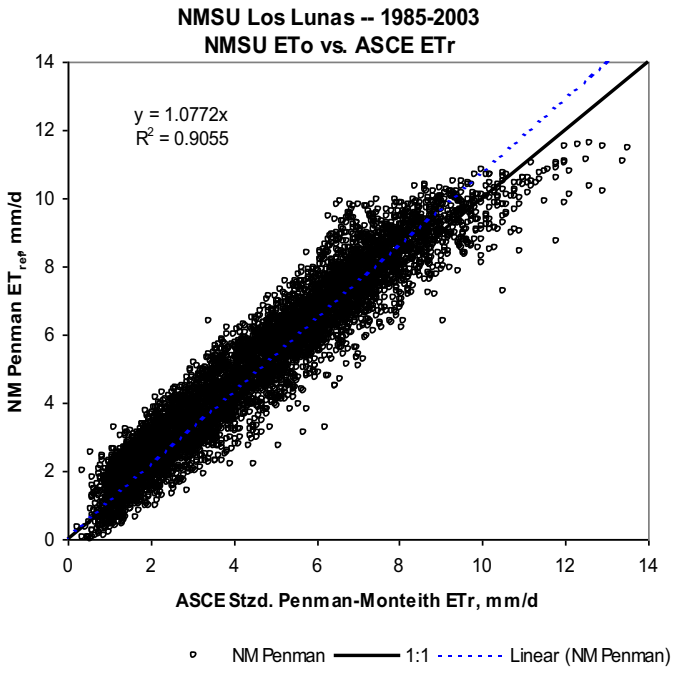

FIGURE 2. Daily "Reference" ET Computed by the New Mexico State University Penman Equation (of ET Toolbox) *vs.* Daily Alfalfa Reference ET Computed by the ASCE-EWRI (2005) Standardized Penman-Monteith Equation for 18 Years of Weather Data Collected at the NMSU Los Lunas Experiment Station (Allen *et al.*, 2008a).

Equation (7) was used to calculate the ET Toolbox ET-based forecasts for "today" and the following six days. The $ET_{o\text{-}NMSU}$ was calculated using weather data from a network of seven weather stations in MRGCD (Brower, 2008) as well as weather forecast parameters provided by the National Digital Forecast Database (*accessed* August 30, 2011, http://www.nws.noaa.gov/ndfd/). The daily assignment of a crop coefficient ($K_{c\text{-}NMSU}$) for each grid cell in the MRGCD was based on its land cover. Prior to June 8, 2004, the Middle Rio Grande Land Use Trend Analysis of 1992/93 (U.S. Bureau of Reclamation, 1997) was used as the land cover database. After that date, a high-resolution land cover map was produced using a combination of July 2000 IKONOS satellite imagery at 4 m resolution and 2001 Utah State University aerial photography at 0.5 m. That high-resolution land cover map was transposed to the grid cell map of ET Toolbox to determine acreage of each agricultural crop (Alfalfa, Corn, Pasture, Orchard, etc.), each type of riparian vegetation (Cottonwood, Salt Cedar, Russian Olive, etc.), and open water in each 1 × 1 km grid cell. As a consequence, the ET Toolbox land cover map generally was at least several years out of date. In this study for the year 2007, the land cover map was approximately six years old.

Important features in the ET Toolbox are the dates when a land cover is assumed to become active and ET begins, and when the area becomes inactive and ET stops. For example, corn was assumed to begin its growth phase starting on April 29, and remain active until November 20. Thus, a field classified on the imagery of 2001 as Corn would, in 2007, be estimated to consume water during six months and 22 days out of the year, with zero ET in the remaining period. Of course, in 2007, a field may actually be planted with alfalfa, which has a growing season from January 1 through October 20, or it may be bare, i.e., considered in ET Toolbox as inactive with zero ET, but underlain by a shallow groundwater table that almost certainly maintains a small soil evaporation rate (Hendrickx *et al.*, 2003). To mitigate the issue of out-of-date land cover maps, MRGCD switched, in 2012, to the use of crop reports developed from field surveys performed by ditch riders throughout the irrigation season so that the ET Toolbox now uses one-year-old land cover data. In this context, it is relevant to observe that no land cover data are needed for ET predictions using the SEBAL/METRIC approach (Allen *et al.*, 2011), although land cover information may somewhat increase the accuracy of ET predictions by improving estimates of the surface roughness of each cell.

The width of the Middle Rio Grande Valley varies from less than 1 km to about 8 km. As a result, there are many edge cells located on the boundary between low-lying valley lands and higher dry upland terrain. These boundary cells cover the area that remains between the last full-sized cell and the boundary between the floodplain and desert up-lands. As a consequence, many of these cells are considerably smaller than 1 km^2 which may lead to inaccuracies when re-projecting different data layers to a common projection and, therefore, they have been eliminated. As a result, all of our analyses are based on 831 approximately 1 × 1 km cells that are entirely located in the valley and mostly underlain by a shallow (0-5 m) groundwater table (Bexfield and Anderholm, 1997; S.S. Papadopulos & Associates, Inc., 2006).

The performance indicator, total annual ET for 2007, using the traditional ET Toolbox approach without MODIS imagery ($ET_{Kc\text{-}NMSU}$) was calculated in this study using:

$$ET_{K_c\text{–}NMSU} = \sum_{day=1}^{day=365} \sum_{cell=1}^{cell=831} (K_{c-NMSU} \times ET_{o-NMSU})/831 \quad (8)$$

In contrast, the performance indicators based on the ETrF maps generated by METRIC from MODIS imagery were not based on the New Mexico State University Penman reference ET, $ET_{o\text{-}NMSU}$, but on the ASCE standardized Penman-Monteith equation for the alfalfa reference, ET*r* (Allen *et al.*, 2007a). Because the data presented in Figure 2 suggest that

$$ET_{o-NMSU} = 1.077 \times ET_r \quad (9)$$

we developed a METRIC-derived crop coefficient ($K_{c\text{-}METRIC}$) to be used with $ET_{o\text{-}NMSU}$ as

$$K_{c-METRIC} = \frac{ETrF}{1.077} \quad (10)$$

and the performance indicator using METRIC ETrF inside the ET Toolbox ($ET_{Kc\text{-}METRIC}$) as

$$ET_{K_{c-METRIC}} = \sum_{day=1}^{day=365} \sum_{cell=1}^{cell=831} (K_{c-METRIC} \times ET_{o-NMSU})/831 \quad (11)$$

The primary difference between Equations (8) and (11) are that Equation (8) uses "static" K_c values developed by NMSU, and Equation (11) uses spatially varying K_c values developed from the METRIC application. The daily ETrF values were determined by linear interpolation between the ETrF images derived from the 26 MODIS images to simulate common interpolation practice.

The performance indicator based on METRIC only without using ET Toolbox (ET_{METRIC}) was calculated as

$$ET_{METRIC} = \sum_{day=1}^{day=365} \sum_{cell=1}^{cell=831} (ETrF \times ET_r)/831 \quad (12)$$

where ET_r was computed using the ASCE standardized Penman-Monteith equation and ETrF was produced from the METRIC process. The daily ETrF values of this performance indicator were not determined by linear interpolation but by fitting a spline between the ETrF images derived from the 26 MODIS images, which follows common METRIC practice (Allen *et al.*, 2007a). In general, the spline function tends to more smoothly follow the evolution of ETrF caused by evolution in vegetation development, than does a linear interpolation. In addition, the convex nature of ETrF *vs*. time of growing season tends to cause the linear interpolation to understate total ET due to undercutting of the convex curvilinear ETrF time-based curve (Allen *et al.*, 2007a). In METRIC, the quality controlled measurements at the two representative automated weather stations of Angostura and Boys Ranch were used for the calculation of an average daily ET_r for all 831 cells (Allen *et al.*, 2008a). The annual sum of these daily ET_r values was 1,950 mm and ideally this number should be similar to the annual ET_r that contributed to performance parameter $ET_{Kc\text{-}METRIC}$. One can insert Equations (9) and (10) into Equation (11) to confirm this. However, due to uncertainty of regression Equation (9) as well as the use of seven instead of two weather stations and spatial weighting schemes for assigning a reference $ET_{o\text{-}NMSU}$ to each grid cell in ET Toolbox, the annual ET_r for performance indicator $ET_{Kc\text{-}METRIC}$ was 1,767 mm, or about 10% less than the 1,950 mm for performance indicator ET_{METRIC}.

To benchmark the three different performance indicators ($ET_{Kc\text{-}NMSU}$, $ET_{Kc\text{-}METRIC}$, ET_{METRIC}) against each other, we not only used their averages over 831 cells but also their averages over different land covers. We calculated the values for the performance indicators for each land cover class defined in 2008 by the National Agricultural Statistics Service (NASS) of the U.S. Department of Agriculture (http://nassgeodata.gmu.edu/CropScape/, *accessed* September 10, 2012). The land covers consisted of agricultural crops (corn, sorghum, winter wheat, alfalfa, pecans), fallow land, and nonagricultural classes similar to the ones used in the 2006 National Land Cover Database (Fry *et al.*, 2011). All data were downloaded at a spatial resolution of 57 × 57 m. We used the 2008 NASS dataset as it was the first year available and sufficiently close to 2007 to identify the

irrigated areas and other major land covers in the MRGCD. We then reclassified all agricultural crops into one new class of "irrigated lands." Before using these data, we aggregated the 57 × 57 m cells into 1,000 × 1,000 m cells assigning the land cover occurring with the highest frequency to the aggregated cells. For example, if 51% of the 57 × 57 m cells in one 1,000 × 1,000 m cell were "shrubland" and 49% were "irrigated land," then the aggregated cell would be classified as "shrubland." This aggregation process introduced considerable bias for many pixels, as the subpixel-scale variability of heat fluxes in the MRGCD was quite high (Kleissl *et al.*, 2009). Overall, the total ET aggregated over all 831 pixels of 1,000 × 1,000 m was assumed to have much lower bias than for individual pixels, due to randomized assignment of majority land use type on a pixel-by-pixel basis. The result would be cancellation of error in proportion to the square root of the number of cells, or a reduction of $831^{0.5}$ or about 29 times. The eight land cover classes were: Open Water (WAT), Woody Wetlands (WWE), Irrigated Land (IRR), Pasture/Hay (PAS), Grassland Herbaceous (GRA), Shrubland (SHR), Developed/Open Space (DEO), and Developed/Low intensity (DEL) (Table 3).

Benchmark Results for ET Toolbox

Table 3 presents the total annual ETs in 2007 estimated using ET Toolbox in its traditional way and with METRIC ETrFs. The average annual 2007 ET performance indicators — $ET_{Kc\text{-}NMSU}$, $ET_{Kc\text{-}METRIC}$, and ET_{METRIC} — were 543, 771, and 832 mm, respectively, over the 831 cells. The absolute and relative differences of (832-771=) 61 mm and 8% between the average $ET_{Kc\text{-}METRIC}$ and ET_{METRIC} was not expected as according to Equations (9)-(12) these performance indicators should have approximately the same value. This difference appears primarily caused by the interpolation method of the ETrF images for calculation of the ET performance indicator, linear interpolation for $ET_{Kc\text{-}METRIC}$, and the more accurate spline interpolation for ET_{METRIC} (Allen *et al.*, 2007a). A secondary possible cause is that the reference ETs used for the calculations of $ET_{Kc\text{-}METRIC}$ and ET_{METRIC} were based on data from different weather stations as explained in the previous section. The 8% difference is considered to be within the commonly accepted uncertainty of remotely sensed ET (Karimi and Bastiaanssen, 2015).

Because ET_{Kc_NMSU} and $ET_{Kc\text{-}METRIC}$ are both results of ET Toolbox, we focused our benchmark analysis on these two performance indicators. The absolute and relative differences between $ET_{Kc\text{-}NMSU}$ and $ET_{Kc\text{-}METRIC}$ for all 831 cells were (771-543=) 228 mm and 30%. This is a large difference; however, one should keep in mind that the purpose of the traditional ET Toolbox is to estimate crop and riparian vegetation ET from "active" areas and open water evaporation within specified river reaches (Brower, 2008). The ET Toolbox was not developed to estimate ET from all areas, including what are classified by USBR as "inactive" areas that contain desert shrubs or bare soils, fallow fields, or agricultural fields during winter time. METRIC, on the other hand,

TABLE 3. The Average Annual Actual ET in Case Study I, Its Standard Deviation, and Its Coefficient of Variation for 831 Pixels of About 1 × 1 km for the Three Performance Indicators ($ET_{Kc\text{-}NMSU}$, $ET_{Kc\text{-}METRIC}$, ET_{METRIC}) for All Pixels and for Each Land Cover Class.

Land Cover[1]			Annual ET (mm/yr)			Standard Deviation of Annual ET (mm/yr)			Coefficient of Variation of Annual ET (-)		
	N[2]	AA[3]	$ET_{Kc\text{-}NMSU}$	$ET_{Kc\text{-}METRIC}$	ET_{METRIC}	$ET_{Kc\text{-}NMSU}$	$ET_{Kc\text{-}METRIC}$	ET_{METRIC}	$ET_{Kc\text{-}NMSU}$	$ET_{Kc\text{-}METRIC}$	ET_{METRIC}
ALL	831	40	543	771	832	246	205	230	45	27	28
WWE	123	40	621 B[4]	898 A	978 AB	199	188	170	32	21	17
WAT	38	41	605 B	878 AB	1,029 A	216	179	161	36	20	16
IRR	60	52	707 A	863 ABC	927 BC	155	158	172	22	18	19
PAS	178	41	632 AB	830 BCD	892 CD	185	166	178	29	20	20
GRA	35	44	640 AB	804 CD	790 EF	252	145	155	39	18	20
DEO	57	43	566 B	768 D	838 DE	223	193	207	39	25	25
SHR	260	36	439 C	700 E	744 F	258	176	244	59	25	33
DEL	80	31	355 D	545 F	616 G	230	201	179	65	37	29

[1]WWE, Woody Wetlands; WAT, Open Water; IRR, Irrigated Lands; PAS, Pasture/Hay; GRA, Grassland Herbaceous; DEO, Developed/Open Space; SHR, Shrubland; DEL, Developed/Low Intensity.
[2]N is number of 1,000 × 1,000 m cells present in each land cover class.
[3]The Active Area is the percentage of a pixel area where ET takes place; the Inactive Area is the percentage of a pixel area with bare and sparsely vegetated spots where ET Toolbox assumes zero ET. AA is annual mean active area used for the calculation of $ET_{Kc\text{-}NMSU}$ in the traditional ET Toolbox. The AA of IRR is significantly higher than all other classes; the AAs of WWE, WAT, and SHR are not significantly different.
[4]Values with a different letter are significantly different at the 5% significance level. For example, ET_{METRIC} values of Open Water (WAT) and Irrigated Lands (IRR) are significantly different because they do have different letters, respectively, an A and a B.

estimates a spatially continuous ET field over an entire region or watershed including shrubs and bare soils having low ET rates. For that reason it is to be expected that the cumulative ET derived from METRIC is higher than that estimated from the traditional ET Toolbox approach. Neither approach is necessarily "right" or "wrong," as they are designed to detect or estimate the ET from different areas of interest.

Table 3 also presents the $ET_{Kc\text{-}NMSU}$, $ET_{Kc\text{-}METRIC}$, and ET_{METRIC} for the eight land cover classes. An analysis of variance was conducted to test whether differences among $ET_{Kc\text{-}NMSU}$, $ET_{Kc\text{-}METRIC}$, and ET_{METRIC} depend on land cover. All three performance indicators did significantly ($p < 0.001$) depend on land cover but only a small part of their variability was explained by land cover as expressed in the R^2-values of 20, 26, and 25% for, respectively, $ET_{Kc\text{-}NMSU}$, $ET_{Kc\text{-}METRIC}$, and ET_{METRIC}. These low R^2-values were expected as (1) previous research demonstrated a large variability of heat fluxes within cells having dimensions of 1,000 × 1,000 m (Kleissl *et al.*, 2009); and (2) the NASS land cover classes do not capture well the true differences in land cover of an arid floodplain in New Mexico at a scale of 1,000 m. For example, visual false color image-based inspection of the land types occurring in land cover classes Pasture/Hay (PAS), Grassland Herbaceous (GRA), Developed/Open Space (DEO), and Developed/Low Intensity (DEL) revealed that they do contain irrigated parcels. For that reason we did not further consider these four land cover classes, but instead, focused our discussion on Open Water (WAT), Woody Wetlands (WWE), Irrigated Lands (IRR), and Shrubland (SHR) that represent truly different environments in MRGCD. Indeed, land cover Shrubland was significantly different from all other land covers for $ET_{Kc\text{-}NMSU}$ and $ET_{Kc\text{-}METRIC}$, but cannot be distinguished significantly from Pasture/Hay for ET_{METRIC}. The land cover classes Woody Wetlands and Open Water were not significantly different for any of the three performance indicators, but together they represented the moist nonagricultural areas covering the river and adjacent wetlands.

The $ET_{Kc\text{-}METRIC}$ values were ranked from highest to lowest as they explain most of the variability caused by land cover; $ET_{Kc\text{-}NMSU}$ and ET_{METRIC} values followed this ranking in Table 3. The highest annual $ET_{Kc\text{-}METRIC}$ occurred in cells classified as Woody Wetlands with 898 mm, Open Water with 878 mm, and Irrigated Lands with 863 mm, but these values were not significantly different. The 700 mm value of Shrubland was significantly lower. A completely different ranking was found for $ET_{Kc\text{-}NMSU}$ with the highest value of 707 mm in Irrigated Lands and significantly lower values of 621 and 605 mm in Woody Wetlands and Open Water, respectively. Again, Shrubland was significantly lower with 439 mm. The ranking of ET_{METRIC} basically followed the one of $ET_{Kc\text{-}METRIC}$ with values of 978, 1029, and 927 mm for, respectively, Woody Wetlands, Open Water, and Irrigated Lands. Shrubland was the lowest with 744 mm.

The absolute and relative differences between $ET_{Kc\text{-}METRIC}$ and ET_{METRIC} for Woody Wetlands and Open Water cells were, respectively, 80/151 mm and 8/15%; for Irrigated Lands, the values are 64 mm and 7% and for Shrubland 44 mm and 6%. These values confirmed that the differences between $ET_{Kc\text{-}METRIC}$ and ET_{METRIC} are minor and mainly caused by their different approaches for calculation of the reference ET_r as discussed before. The absolute and relative differences between $ET_{Kc\text{-}NMSU}$ and $ET_{Kc\text{-}METRIC}$ for Woody Wetlands and Open Water cells were, respectively, 277/273 mm and 31/31% while for Irrigated Lands these values were 156 mm and 18% and for Shrubland 261 mm and 37%. The standard deviations of $ET_{Kc\text{-}NMSU}$ and $ET_{Kc\text{-}METRIC}$ for Woody Wetlands, Open Water, Irrigated Lands, and Shrubland were, respectively, 199/188 mm, 216/179 mm, 155/158 mm, and 258/176 mm, and the respective coefficients of variation were 32/21%, 36/20%, 22/18%, and 59/25%. The overall picture that arises from the magnitude of these differences is that the performance parameters $ET_{Kc\text{-}NMSU}$ and $ET_{Kc\text{-}METRIC}$ for land cover class Irrigated Lands were more similar than for other classes. Not only were their absolute and relative ET differences of 156 mm and 18% smaller than those of Woody Wetlands, Open Water, and Shrubland, but also their standard deviations and coefficients of variation were nearly the same and the lowest among the land cover classes. The difference of 156 mm between performance parameters $ET_{Kc\text{-}NMSU}$ and $ET_{Kc\text{-}METRIC}$ for land cover class Irrigated Lands is most likely largely due to capillary rise and bare soil evaporation during the winter season when ET Toolbox assumes evaporation to be zero on inactive lands, whereas the thermally based energy balance of METRIC was able to detect evaporation from wet soil. METRIC-based ET was aggregated over the calendar year to demonstrate the positive impact of considering evaporation and ET during all parts of the year. On average, during 2007, the active area of Irrigated Lands cells was 52% (Table 3), leaving 48% as inactive. As groundwater table depths in the floodplain of the Rio Grande are shallow (0-5 m below surface) (S.S. Papadopulos & Associates, Inc., 2006) and the soils generally have a medium to fine texture (Nelson *et al.*, 1914), capillary fluxes can vary from more than 1 mm/day to close to zero (Hendrickx *et al.*, 2003). Such fluxes could explain part of the ET difference of 156 mm between the traditional and

METRIC approaches. Yet, another reason for the discrepancy may be that the land use map used by ET Toolbox was more than six years old so that erroneous land use classes may have affected the total annual ET estimation.

The dynamics of performance parameters $ET_{Kc\text{-}NMSU}$ and $ET_{Kc\text{-}METRIC}$ for land cover classes Woody Wetlands, Open Water, and Shrubland were quite different. The absolute and relative differences between $ET_{Kc\text{-}NMSU}$ and $ET_{Kc\text{-}METRIC}$ were much larger than the 156 mm and 18% found in land cover Irrigated Lands; they were, respectively, 273, 277, and 261 mm, and 31, 31, and 31%. As for the irrigated lands, the differences in ET were most likely due to capillary rise and bare soil evaporation, not only during the winter season when ET Toolbox assumes evaporation to be zero, but also during the growing season on the bare soil patches that are typical of the riparian and shrub areas. The mean average active areas of Woody Wetlands, Open Water, and Shrubland were 39% so that their total inactive area, i.e., bare and sparsely vegetated spots where ET was set equal to zero, and is 61% or about 25% more than the 48% of Irrigated Lands. As explained earlier, capillary fluxes on inactive areas can make up part of the ET difference of 261-277 mm between the traditional and METRIC approaches for Woody Wetlands, Open Water, and Shrubland. Yet, another reason for the discrepancy may be the six-year-old land use map as discussed in the previous paragraph and the lack of a majority of any particular land use type in a 4 km grid cell, thereby impacting accuracy of the $ET_{Kc\text{-}NMSU}$ estimates.

The sharp decrease in the standard deviations and coefficients of variation is another characteristic of the statistics in Woody Wetlands, Open Water, and Shrubland (Table 3) when the traditional ET Toolbox approach was replaced by a METRIC-based one. While the standard deviation and coefficient of variation of Irrigated Lands for $ET_{Kc\text{-}NMSU}$ and $ET_{Kc\text{-}METRIC}$ basically remained the same, the standard deviation of Woody Wetlands, Open Water, and Shrubland decreased by, respectively, 11, 37, and 82 mm; coefficients of variation decreased from 32 to 21%, 36 to 20%, and 59 to 25%. Therefore, the standard deviations and coefficients of variations for Woody Wetlands, Open Water, and Shrubland approached those of Irrigated Lands or — in other words — the accuracy of annual ET estimates for these classes improved when METRIC was used. On the other hand, METRIC does not need annually varying land cover information as it directly determines the components of the energy balance. Another important factor explaining the higher accuracy of METRIC is that it captures, not only in active areas, but also in inactive areas, the change in soil evaporation and riparian vegetation transpiration due to capillary fluxes as a result of groundwater depth change between years and during a water year. Many studies have confirmed that groundwater depth is an important factor affecting ET, particularly in riparian and groundwater discharge areas with phreatic vegetation (White, 1932; Van Hylckama, 1974; Moayyad *et al.*, 2003; Shafike *et al.*, 2007). For example, Van Hylckama (1974) studied water use by salt cedar, a phreatophyte known to utilize groundwater, during a seven year period using lysimeters and found that the plant's ET rate was highly dependent on the depth to groundwater, with 2,150 mm/yr with depth of 1.5 m decreasing to less than 1,000 mm/yr for depth of 2.7 m.

A final aspect considered is whether METRIC applied with MODIS imagery yields accurate ET values. Previous studies have found generally good agreement between METRIC ET derived from MODIS compared with up-scaled Landsat ET maps (Allen *et al.*, 2008b; Hong *et al.*, 2009, 2011a). In addition, eddy-covariance ET measurements and HYDRUS1D simulations from 1999 at a flooded Salt Cedar site in the MRGCD yielded an annual ET of 1,120 and 1,140 mm/yr, respectively (Moayyad *et al.*, 2003), which suggests that the ET_{METRIC} value of 1,140 mm from 2007 at that location is accurate.

Benchmark Conclusions for ET Toolbox

Observing the large differences in estimation of annual ET in 2007 for the 831 cells in MRGCD by the three performance indicators $ET_{Kc\text{-}NMSU}$, $ET_{Kc\text{-}METRIC}$, and ET_{METRIC}, and considering the positive METRIC validations with MODIS imagery in the Rio Grande Valley, optical/thermal imagery has the potential to considerably improve the forecasts of ET in the MRGCD. It is very likely that a nearly real-time implementation of METRIC would generate benefits that outweigh the costs of such an operation, especially in light of recent efforts to reduce costs of human oversight and intervention on METRIC and similar model applications (Allen *et al.*, 2013) and implementation of the METRIC algorithms on the very fast Google Earth Engine cloud via an application named EEFlux (Earth Engine Evapotranspiration Flux) (Kilic *et al.*, 2014). All patterns of water use (when, where, and how much) need to be known during the entire year before water can be optimally managed in times of scarcity and drought. This information can only be obtained from the METRIC Landsat-based ET because the ET derived from the ET Toolbox only provides the expected average ET during the growing season under optimal conditions.

CASE STUDY II: GSSHA IN THE KISHWAUKEE WATERSHED

The GSSHA model case study is an example of how optical/thermal imagery can improve model hydrologic predictions through initialization of soil moisture state in the models. GSSHA (Ogden *et al.*, 2000; Downer and Ogden, 2004, 2006) is a two-dimensional, physically based, distributed parameter hydrologic model that simulates a variety of hydrologic processes, including: parameterizations for rainfall interception and infiltration, overland flow retention, ET, surface runoff and subsurface routing. GSSHA is applicable in most watersheds because its formulation includes Richards equation infiltration, two-dimensional implicit groundwater routing, and an optional conceptual base flow model based on the Sacramento Soil Moisture Accounting (SAC-SMA) model. GSSHA is used by the U.S. Army Corps of Engineers not only within the U.S. but also worldwide. GSSHA is public domain software maintained by the U.S. Army Corps of Engineers, Engineering Research and Development Center, and can be downloaded from the GSSHA Wiki (*accessed* August 23, 2014, www.gsshawiki.com/gssha/Gridded_Surface_Subsurface_Hydrologic_Analysis).

An accurate initialization of spatially distributed GSSHA soil moisture is critical when predicting peak discharges and maximum flood levels in rivers of interest on short notice in support of civilian and military operations. In applications without remotely sensed root zone soil moisture, there is little to no time to gather spatially distributed field estimates of the soil moisture conditions needed to initialize GSSHA. In the absence of field data, the model is initialized using an initially uniform soil moisture state such as dry, average, or wet, and running the model from before a previous rainfall recorded event. Errors in initial soil moisture estimates were found to be diminished after a significant rainstorm is simulated (Senarath *et al.*, 2000). However, this process first increases simulation time when time is of the essence and it also results in errors in the peak hydrograph and, thus, the prediction of maximum flood levels. We performed this study to see if improved initial soil moisture estimates significantly improve model performance, as well as increase parameter set uniqueness when calibrating. Therefore, we selected the predicted storm hydrograph as the performance indicator for GSSHA.

Benchmark Approach for GSSHA

For this study, we used GSSHA simulations in the Kishwaukee Watershed. The Kishwaukee River originates near Woodstock, Illinois, and flows to Rockford, Illinois, where it discharges into the Rock River. The watershed covers approximately 3,000 km^2 and contains a dense network of streams with a total length of about 1,600 km. Agricultural lands occupy about 70% of the watershed; the remainder is covered by forests, sloughs, wetlands, and urban areas. GSSHA simulations in the Kishwaukee watershed for the prediction of flood changes caused by land use conversion, removal of tile drains, and installation of a wetland were used as the basis for this study (Byrd, 2013). Average annual precipitation is 950 mm and average annual evaporation is 750 mm (Kay and Trugestaad, 1998).

Discharge measurements were made from April 1, 2002, through October 11, 2002 (Figure 3). Unfortunately, no matching hourly NEXRAD distributed precipitation data were available for this entire period. Therefore, Event 1 and Event 2 (Figure 3) have been split and simulated individually with GSSHA in this proof of concept study; Event 1 started on June 3 and Event 2 on August 21. Hourly NEXRAD distributed precipitation images have been used as input to the GSSHA model.

For our study period, only the Landsat image of June 18, 2002 was of sufficient cloud-free quality to map ET and soil moisture. This image is located in the tail of the hydrograph of Event 1 and is assumed to represent soil moisture conditions typical for periods in the growing season without precipitation as occurred just before Event 1 in early June and Event 2 in late August. A horizontal grid increment of 250 m was used in the simulations, resulting in approximately 48,000 grid cells within the watershed.

We benchmarked the prediction of two hydrographs after the two large storms occurring in June and August 2002 (Events 1 and 2 in Figure 3) using individual GSSHA simulations. Our approach for benchmarking and evaluating the value of using the Landsat-derived soil moisture product for initializing the GSSHA model is a straightforward application of Equation (6). First, GSSHA was run in its traditional manner with uniform initial soil water contents assigned to all cells in the model before running the model from before a previous significant rainfall event. GSSHA was then run for Event 1 in early June and Event 2 in late August using as the initial soil moisture distribution the one that was derived from a SEBAL analysis for the June 18, 2002, Landsat image (Hendrickx *et al.*, 2009). For the Landsat approach, the SEBAL-generated ET map (Figure 4a) was converted into a soil moisture map using Equation (6) while PET was calculated using daily meteorological data (Allen

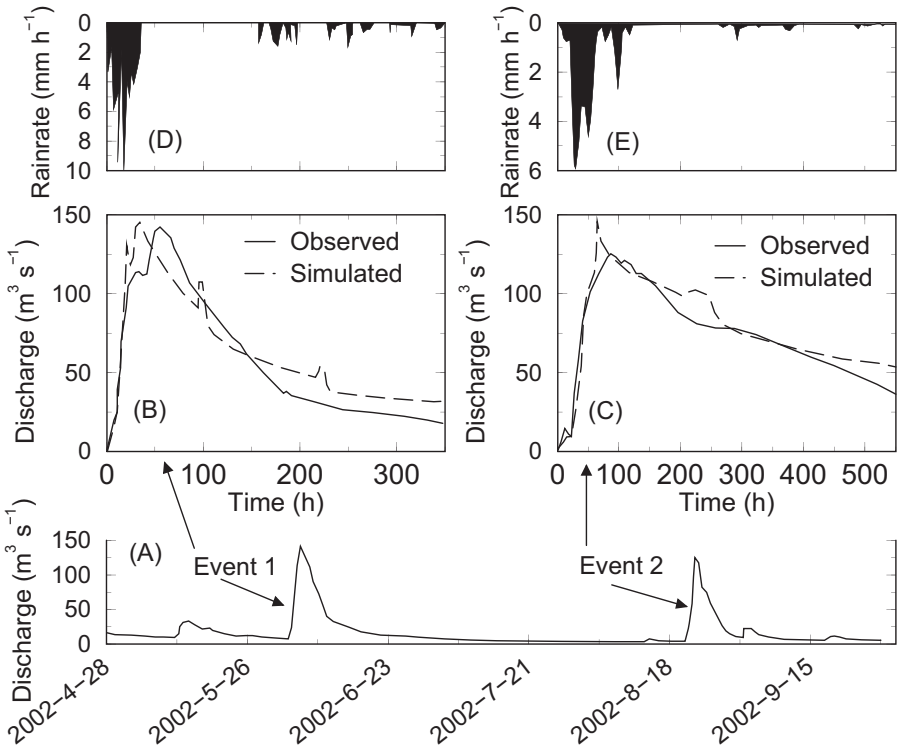

FIGURE 3. Time Series of the Average Radar Precipitation over the Kishwaukee Watershed as well as the Observed and Simulated Discharges at the Outlet of the Kishwaukee Watershed for Event 1 and Event 2 Using the Surface Energy Balance Algorithms for Land-Derived Soil Moisture Map to Initialize GSSHA. The precipitation values shown in this figure are the average values of the distributed radar rainfall over the watershed; in the simulations, the spatially distributed radar rainfall is used so that the cell with the maximum precipitation value receives far more precipitation than the average value (Pradhan *et al.*, 2012).

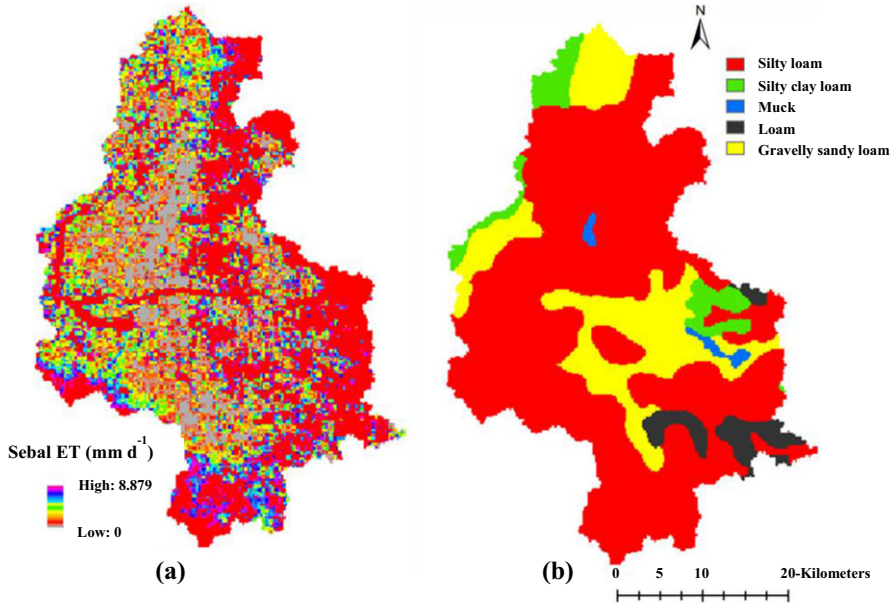

FIGURE 4. Kishwaukee Maps Used for This Study: (a) Surface Energy Balance Algorithms for Land actual ET (mm/day) on June 18, 2002; (b) soils by surface texture (Hendrickx *et al.*, 2009; Pradhan *et al.*, 2012).

et al., 2005d) from a weather station located at 42.11 N, 88.96139 W. For both the traditional and Landsat approaches, the soil map (Figure 4b) was used to determine θ_{wp} and θ_{sat} for each cell in the model using standard USDA soil parameters (Rawls *et al.*, 1982).

No Landsat images were available immediately before the storms of June 3 and August 21, 2002; the only available image was acquired on June 18, 2002, during a period that the discharge in the watershed was at a level somewhat higher than just before Event 1 and Event 2 (Figure 3). In humid regions like the Kishauwkee watershed, only a few clear sky Landsat images are typically available during periods with high rainfall (Sano *et al.*, 2007) and the probability of having a clear sky image just before a major storm event is rather low.

The use of daily MODIS images increases the availability of clear sky images due to the higher frequency of overpass. However, because the thermal band of MODIS has a resolution of 1,000 m, the MODIS ET and soil moisture maps have lower resolution than those of Landsat 5, which has a thermal band resolution of 120 m. This begged the question: What is the value of a soil moisture map obtained from moderate resolution Landsat imagery weeks before or after the storm event to be simulated, compared to a more frequent, but lower-resolution soil map? We hypothesized that the value of a higher resolution but less-frequent soil moisture map would be of considerable value because generally there exists a "temporal persistence of spatial patterns of soil water storage" (Kachanoski and de Jong, 1988) or, more accurately, a "time stability of the rank of individual observations in the probability distribution function of the whole population" (Vachaud *et al.*, 1985) of soil moisture values. The "rank order stability" of soil moisture patterns can be described then as the temporal persistence of spatial soil moisture patterns, i.e., even when the average soil moisture conditions change due to precipitation and ET; the rank order of soil moisture for each cell often will remain relatively unchanged. One important reason for time stability of soil moisture patterns is the strong relationship between soil texture, landscape position, and soil moisture (e.g., Vachaud *et al.*, 1985; Hendrickx *et al.*, 1990; Hillel, 1998; Jury and Horton, 2004). This relationship is so strong that soil boundaries between soil series can be determined using field soil water content measurements (Hendrickx *et al.*, 1986) or series of SEBAL-generated soil moisture maps (Engle *et al.*, 2010, 2014) similar to the map used in this case study. Therefore, we expected that the June 18 SEBAL soil moisture map would reveal soil moisture patterns similar to the ones existing in the watershed just before Event 1 starting on June 3 and Event 2 starting on August 21. If true, then the June 18 soil moisture map would be a better option for initialization of GSSHA than an artificial, spatially uniform soil moisture distribution, or lower resolution MODIS soil moisture map.

Benchmark Results for GSSHA

Figure 5 shows for Event 1 how the simulated runoff hydrograph varied with the various uniform initial soil-moisture conditions, which were evaluated with observed discharges using the Nash-Sutcliffe (N-S) efficiency. Table 4 presents for Event 1 the variation of the N-S efficiency, which represents a goodness-of-fit between the observed and simulated hydrographs. The N-S efficiency varies from −0.02 for uniform initial soil moisture of 70% to 0.81 for a uniform initial soil moisture of 40% during the sensitivity analysis and calibration of Kishwaukee watershed. Because discharge measurements are available, we recognize that the uniform 40% initial soil moisture produced the most efficient hydrograph using the traditional GSSHA initialization method. However, the use of the June 18 SEBAL soil moisture map resulted in N-S efficiencies of 0.88 and 0.85 for Events 1 and 2, respectively. This is a strong indication that soil moisture distributions during the period of discharge measurements have a robust rank order stability and that this knowledge substantially improves estimation of individual flood events. Senarath *et al.* (2000) showed that distributed-parameter physically-based hydrologic models are quite sensitive to assumed initial soil moisture values, and this sensitivity destroys the validity of single-event calibrations when assumed values are used. They also showed significant improvements in calibration verification when more realistic soil moistures were simulated. The results shown in Figure 5 and Table 4 clearly show that if SEBAL soil moisture estimates are available, model performance is considerably improved when used to initialize soil moisture.

GSSHA is a fully distributed hydrologic model that accounts for soil moisture conditions in each time step. Therefore, GSSHA can be used not only to predict hydrographs but also to predict real-time soil moisture dynamics in a watershed. Figure 6a presents the June 18, 2002 soil moisture distribution derived from the SEBAL ET map (Figure 4a) using Equation (6). This map was used to initialize the simulations of Events 1 and 2; this map contains substantial spatial details and is much more robust than the soil moisture distributions used for traditional GSSHA simulations. The model-predicted soil moisture distributions 16 days after Event 1 are shown in Figures 6b-6e. Figures 6b-6d show soil moisture distributions initiated with, respectively, 10, 40, and 70% uniform initial water content while Figure 6e shows the soil moisture distribution initiated using the SEBAL June 18-based soil moisture map (Figure 6a). Even after 16 days, the soil moisture maps initialized with uniform initial soil moisture distributions (Figures 6b-6d) still retain unrealistic features

as compared with that produced using the SEBAL-initialized soil moisture map. Figure 6e shows a high spatial variability and much wider variability of soil moistures across the watershed. This latter feature is best seen by comparing the soil moisture density distributions of the simulations (Figure 7). Whereas the simulations initialized with uniform initial soil moisture have their densities concentrated in a rather narrow band, the density distribution resulting from the SEBAL soil moisture map spans a wide range of soil moisture conditions. For initialization with 10, 40, and 70% uniform initial soil moisture, the respective soil moisture values ranged from 0.10-0.17, 0.18-0.34, and 0.20-0.35 while the SEBAL initialization yielded a range of 0.12-0.39.

Benchmark Conclusion for GSSHA

Comparison of the measured hydrographs in this study with the hydrographs simulated with and without using spatially-distributed initial soil moisture state estimate derived from optical/thermal Landsat satellite imagery has established that such imagery has the potential to considerably improve the prediction of hydrographs and river levels using distributed hydrologic models. In addition, we observed that simulated soil moisture distributions exhibit greater variability that seems more natural when satellite imagery was used to initialize the GSSHA model.

This study also demonstrated that in cloudy regions where clear sky Landsat imagery is limited (Asner, 2001; Wohl *et al.*, 2012), the rank order stability of soil moisture patterns enables the use of SEBAL/METRIC-derived soil moisture maps for model initialization on dates that are days, weeks, or possibly even years (albeit in the right season) apart in the future or past from the image day.

TABLE 4. Goodness-of-Fit between Simulated and Observed Hydrographs as a Function of Initial Root Zone Soil Moisture Distribution. The uniform cases refer to Event 1.

Initialization of Soil Moisture	Nash-Sutcliffe Efficiency
Uniform soil moisture content of 10%	0.14
Uniform soil moisture content of 30%	0.63
Uniform soil moisture content of 35%	0.75
Uniform soil moisture content of 40%	0.81
Uniform soil moisture content of 70%	−0.02
SEBAL-distributed soil moisture map: Event 1	0.88
SEBAL-distributed soil moisture map: Event 2	0.85

These conclusions are based on data and measurements covering only two storm events in the Kishwaukee watershed and, therefore, need to be confirmed by more field studies. This study supports another research effort in Africa advocating that in un-gauged watersheds ET and soil moisture maps from the METRIC/SEBAL approach can be used as a means for the calibration of distributed hydrologic models (Winsemius *et al.*, 2008).

CASE STUDY III: DPWM IN THE SAN GABRIEL MOUNTAINS OF CALIFORNIA

The DPWM case study serves as an example of how optical/thermal imagery can improve the estimation of critical parameters in hydrologic models. One such parameter is the "total available water" (TAW) for ET that is critical to the parameterization of operational distributed water balance models that determine actual ET and aquifer recharge (Alley, 1984), quantify feedbacks between soil moisture and climate

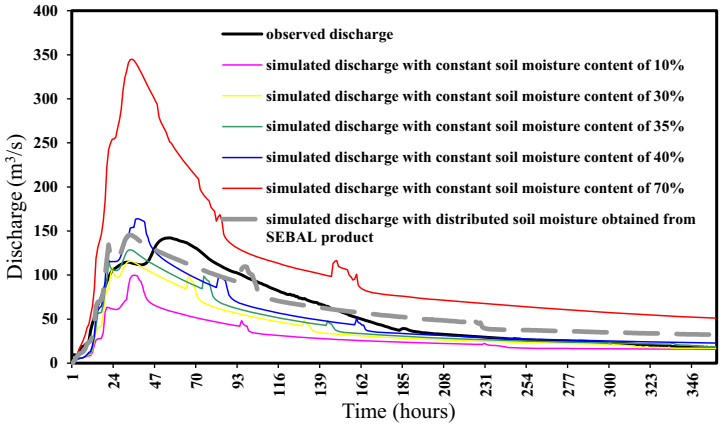

FIGURE 5. Sensitivity Analysis of the Effect of Initial Soil Moisture Distribution on the Difference between Simulated and Observed Hydrographs for Event 1 (Hendrickx *et al.*, 2009; Pradhan *et al.*, 2012).

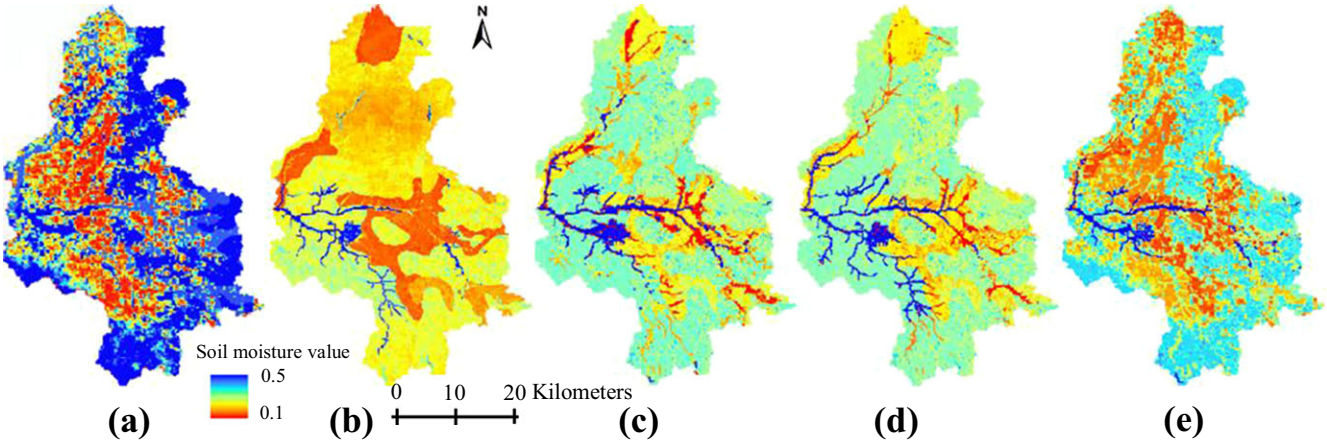

FIGURE 6. Relevant Soil Moisture Maps: (a) Surface Energy Balance Algorithms for Land (SEBAL)-derived soil moisture distribution on June 18, 2002, that is used to initialize the simulations of Event 1 starting on June 3 and Event 2 starting on August 21; GSSHA soil moisture predictions on day 16 of Event, i.e., June 18, starting with uniform initial soil moisture of, respectively, 10% (b), 40% (c), and 70% (d); (e) GSSHA soil moisture prediction on day 16 of Event 1, i.e., June 18, starting with distributed initial soil moisture derived from SEBAL soil moisture map on June 18.

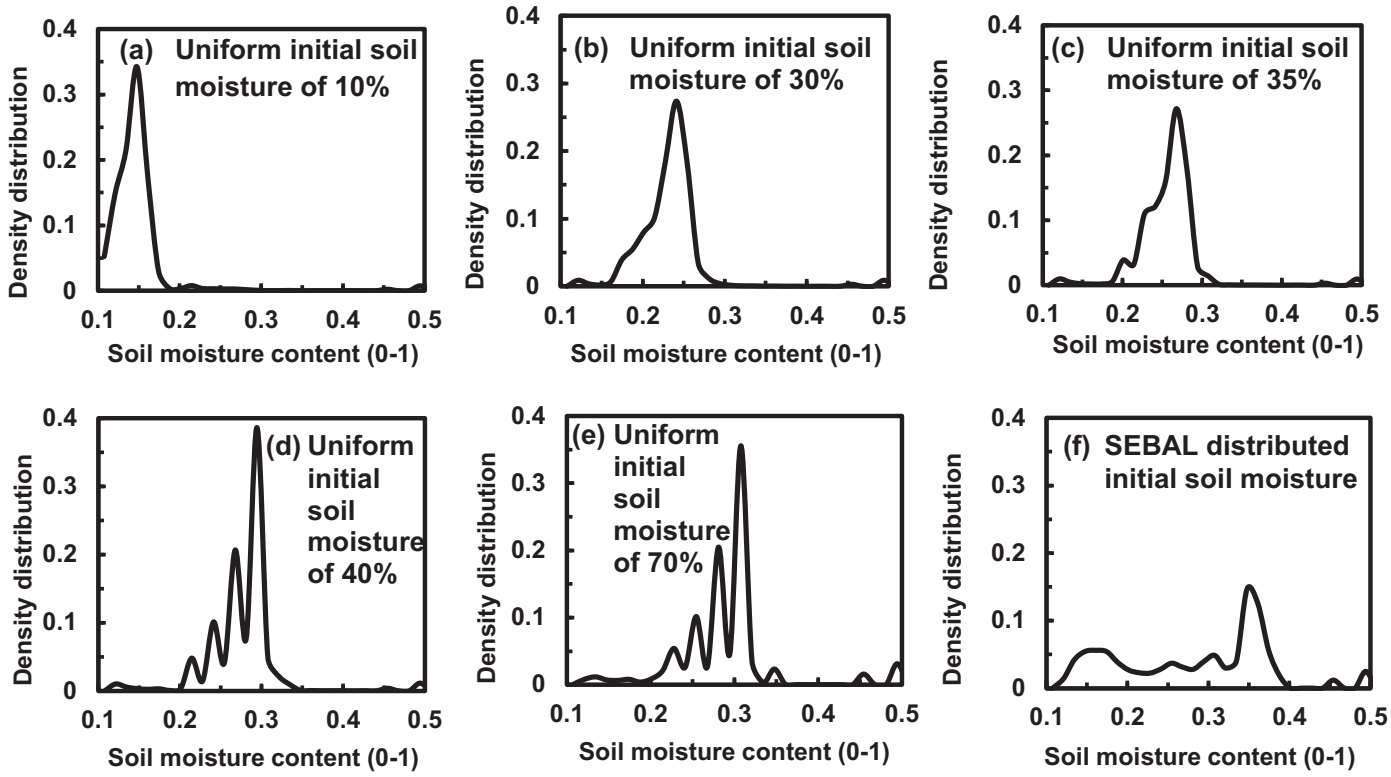

FIGURE 7. Comparison of Soil Moisture Density Distributions on Day 16, i.e., June 18, of the Simulation of Event 1. Each density distribution represents a different initial soil moisture condition. The horizontal axis represents "degree of saturation."

(Seneviratne *et al.*, 2010), estimate runoff (Schaake *et al.*, 1996), assess ET and soil moisture dynamics in ecohydrology (Guswa *et al.*, 2002), and optimize rainfed crop production (Ritchie, 1981b). In DPWM, the parameter TAW is critical to the assessment of groundwater recharge as — on a daily basis — all water added to a soil (precipitation, snowmelt and run-on) in excess of TAW becomes recharge.

DPWM estimates the daily water balance components of precipitation, ET, changes in soil water storage, runoff, recharge, sublimation, and snowmelt at fine-scale resolution within a watershed. The DPWM

is a derivative of the MASSIF model developed by Sandia National Laboratory for the Yucca Mountain Project (Sandia National Laboratory, 2007). All components of MASSIF were developed from publically available, peer-reviewed literature and are primarily based on the United Nations FAO-56 methodology for computing ET (Allen *et al.*, 1998, 2005a, b, c, d). The DPWM improved on MASSIF and generalized the model application to areas outside of Yucca Mountain. Improvements include the following: (1) allowing for variable-sized grid cells for simulating concentrated surface water flow in ephemeral streams; (2) allowing for precipitation model data as input (e.g., PRISM, PERSIANN, or HRLDAS); (3) additional options for snowmelt and sublimation based on the HELP and INFIL model (Schroeder *et al.*, 1994; U.S. Geological Survey, 2008); and (4) incorporation of METRIC satellite data (Allen *et al.*, 2007a, b). DBS&A has applied DPWM to numerous basins in California, Nevada, and New Mexico for the determination of water rights and to estimate recharge and ET in groundwater models (Daniel B. Stephens & Associates, Inc., 2008, 2010a, b, 2011). METRIC has been incorporated in DPWM in the Salt Basin of New Mexico, the Clover Basin of Nevada, and the San Gabriel Mountains in California.

DPWM is a "second-generation" biophysical land surface model (Seneviratne *et al.*, 2010) that takes into account a storage reservoir for evaporation near the surface and one for transpiration from the root zone. Validation of the FAO-56 methodology against weighing lysimeter data and the water balance of the Imperial Irrigation District in California as well as against simulations with the HYDRUS model based on the Richards' equation (Šimunek *et al.*, 2008) demonstrated its strength to produce good estimates of evaporation from bare soils and transpiration from partial or full vegetation covers in agricultural lands (Allen *et al.*, 1998, 2005a, b, c; Allen, 2011). A DPWM validation for semiarid rangeland in southern New Mexico using 27 years of monthly soil water content measurements with the neutron probe to a depth of 130 cm showed that DPWM can adequately simulate observed root zone soil moisture dynamics at a point (Figure 8). These results as well as many other successful applications of relatively simple water balance models in the literature (Vereecken *et al.*, 2008; Seneviratne *et al.*, 2010) indicate that the physical basis of DPWM is rigorous and that it produces realistic representations of soil moisture dynamics and deep percolation if the model can be parameterized correctly.

This case study is conducted in the San Gabriel Mountains that are a fault-bounded mountain block north of the Los Angeles basin and south of the Antelope Valley. The mountains are primarily composed of granitic rocks with some marine sedimentary deposits in the northwest section of the block. Elevations range up to 3,069 m and snow is common at the highest elevations in winter months. Vegetation ranges from desert scrub where the mountain front meets the adjoining valleys to chaparral in the middle elevations up to large conifers at the highest elevations. Recharge from the San Gabriel Mountains provides groundwater to Antelope Valley to the north and to the Los Angeles basin to the south. Precipitation ranges from a mean annual rate of 1,400 mm at the mountain peaks down to 250 mm at the mountain front.

DPWM in its traditional application is parameterized using publically available data from the internet including the USDA SSURGO soils database, USGS GAP database on vegetation, USGS Digital Elevation Model (DEM), MODIS satellite data on vegetation cover, and USGS bedrock geology. Climate data were obtained from local weather stations and then spatially distributed over the model domain based on the PRISM algorithm. As the main purpose of DPWM is the prediction of long-term recharge rates, we selected the average annual groundwater recharge rate as the performance indicator for DPWM.

Benchmark Approach for DPWM

Benchmarking of DPWM was conducted by comparing the average annual groundwater recharge during 1980-2009 in the San Gabriel Mountains after calibration with Landsat-based METRIC and streamflow data to the recharge after calibration with streamflow data only, i.e., the traditional DPWM implementation. DPWM was calibrated to the METRIC data by adjusting in each cell the TAW for ET. The TAW is a permanent soil property for each cell; it is typically defined as

$$\mathrm{TAW} = \left(\theta_{\mathrm{fc}} - \theta_{\mathrm{wp}}\right) \times Z_{\mathrm{R}} \tag{13}$$

where θ_{fc} and θ_{wp} are the volumetric water contents at field capacity and wilting point in the root zone or evaporation zone, respectively, and Z_{R} is the rooting depth or the depth of the bare soil evaporation layer (e.g., Manabe, 1969; Allen *et al.*, 1998; Hillel, 1998; Romano and Santini, 2002; Kirkham, 2005). Equation (13) or variations thereof are often the method of choice for the assessment of TAW in distributed hydrologic models (Flint and Flint, 2007; Hyndman *et al.*, 2007; Sandia National Laboratory, 2007; U.S. Geological Survey, 2008; Daniel B. Stephens & Associates, Inc., 2010a) or in land data assimilation systems (Manabe, 1969; Sellers *et al.*, 1997; Seneviratne *et al.*, 2010). The equation is attractive as digitized

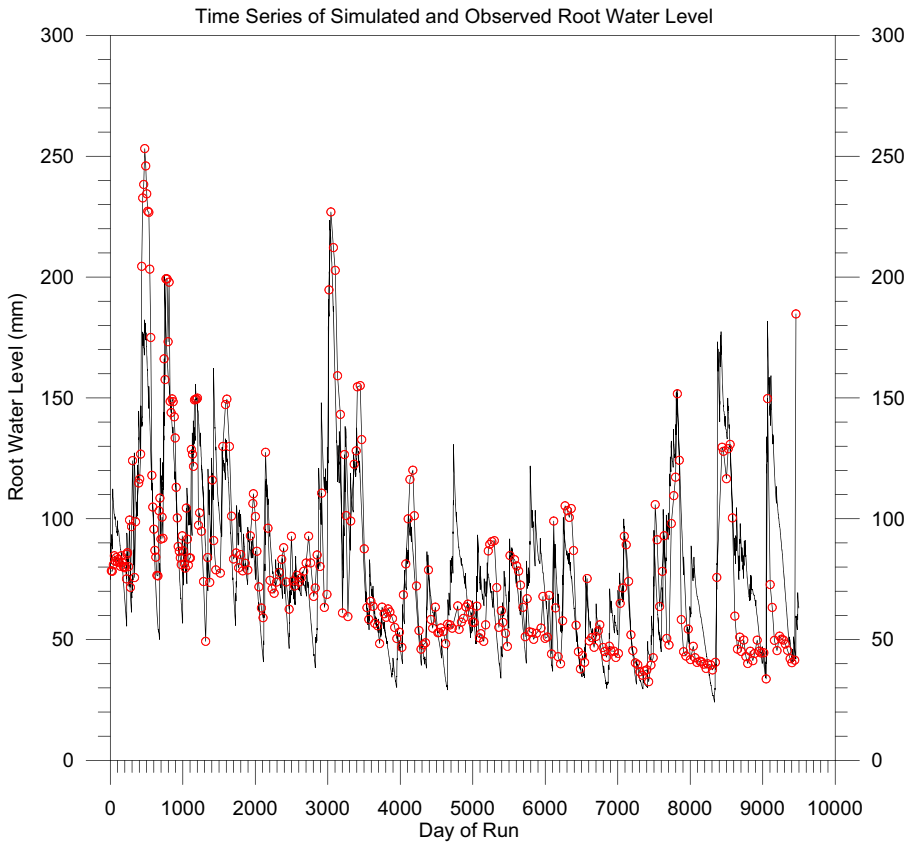

FIGURE 8. Comparison of Neutron Probe Measured (solid line) Versus Distributed Parameter Watershed Model (DPWM) Simulated (open circles) Root Zone Water Storage at a Desert Scrub Access Tube (C18) of the Jornada LTER Transect in New Mexico. The analysis shows that DPWM can simulate the long-term downward trend seen in the observed data as well as short-term changes in soil water increases following large precipitation events. Some discrepancies exist due to model error and/or measurement errors. The monthly measurements may miss peak increases in soil water in the top layer due to smaller rain storms; the neutron probe cannot measure soil water content well near the soil surface. Personal communication by Todd Umstot, November 2011.

geo-referenced soil and vegetation databases can be downloaded for determination of *field capacity* and *wilting point* as well as the *rooting depth* for each cell of distributed models. Soil data are provided by the Soil Survey Staff at the Natural Resources Conservation Service of the United States Department of Agriculture. The Soil Survey Geographic (SSURGO) Database for each state and the U.S. General Soil Map (STATSGO2) are available online at http://websoilsurvey.sc.egov.usda.gov/App/HomePage.htm (*accessed* June 15, 2015). USGS Land Cover Data are available at http://landcover.usgs.gov/usgslandcover.php and http://gapanalysis.usgs.gov (*accessed* June 15, 2015).

However, the simplicity of Equation (13) is deceptive because it is based on assumptions that have validity in deep homogeneous agricultural soils, but not in complex mountainous terrains. Field observations in the San Gabriel Mountains immediately revealed that roots search for water not only in well-defined soils but also in fractured bedrock; more advanced techniques even found enhanced vegetation water uptake by ectomycorrhizal fungi extending from bedrock roots (Allen, 2006). Bornyasz *et al.* (2005) estimated that in shallow soils on southern California hillsides plants extract as much as 86% of their water from the granite bedrock below the soil (Bornyasz *et al.*, 2005). Therefore, in shallow mountain soils barely covering fractured bedrock, the parameterization of Equation (13) using only soil and vegetation databases will result in a large bias in TAW and consequently significantly impact the simulation of ET, runoff, and deep percolation (Laio *et al.*, 2002; Rodriguez-Iturbe and Porporato, 2004).

Another assumption is that volumetric soil water content at *field capacity* and *wilting point* can be accurately derived from laboratory measurements or from information available in soil databases. However, these two terms are not well defined: *field capacity* is the "content of water remaining in a soil two or three days after having been wetted with water and after free drainage is negligible" and *wilt-*

ing point is "water content of a soil when indicator plants growing in that soil wilt and fail to recover when placed in a humid chamber" (Soil Science Glossary Terms Committee, 2008). Field capacity is influenced by many factors: soil texture, type of clay minerals, organic matter content, soil structure, depth of wetting, previous water content, presence of impeding layers in the profile, ET, water table depth, and temperature (Ritchie, 1981a, b; Ratliff *et al.*, 1983; Hillel, 1998; Kirkham, 2005). In the literature, soil water pressures of −330 cm and −100 cm have been typically used to identify field capacity but field capacities are reported to vary from −600 cm in a deep dryland soil to −5 cm in a highly stratified soil (Kirkham, 2005). Field capacities should be measured in the field as the effects of soil layering and hysteresis are difficult to mimic in the laboratory (Ratliff *et al.*, 1983; Cassel and Nielsen, 1986; Romano and Santini, 2002). In addition, there exists no definitive correlation between field capacity and soil texture (Bouma and Droogers, 1999; Ritchie *et al.*, 1999), nor is there justification to associate field capacity with a specific soil water pressure (Stein *et al.*, 2004). The wilting point is also a dynamic variable as it depends on the soil profile (soil texture, compaction, stratification), soil water contents, and root distributions at different depth, transpiration rate of the plant, temperature (Kirkham, 2005), and vegetation type (Hupet *et al.*, 2005; Seneviratne *et al.*, 2010).

The third assumption that the effective depth for root water uptake can be determined from field observations in soil pits may apply to agricultural fields with relatively shallow rooting depths but will fail in complex terrain due to the challenges of soil and root sampling at depth, and the difficulty of estimating *in situ* root activity over the entire root zone (Jackson *et al.*, 2000; Feddes *et al.*, 2001). In Australia, active soil depths, i.e., rooting depths, for agricultural crops, grass, and fallow based on field measurements of extractable water generally varied between 1 and 2 m, while those of trees are more variable ranging from 1 to 12 m, but active soil depths of 5 m were measured for crops and grass on deep sandy soils (Ladson *et al.*, 2006). In eastern Amazonia, water stored at 2-8 m soil depth contributed more than 75% of water uptake not only in forest but also in degraded pasture with deep-rooted woody plants during the severe dry season of 1992 (Nepstad *et al.*, 1994). Clearly, in mountainous areas where shallow soils force the roots to search for water in bedrock cracks, direct field observations for estimation of effective rooting depths are nearly impossible.

As the three assumptions needed for the use of Equation (13) are rarely met in complex terrain or even in agricultural areas, general consensus exists that instead of using some form of Equation (13) the TAW is best measured directly in the field (Israelsen and West, 1922; Ritchie, 1981a, b; Ratliff *et al.*, 1983; Hillel, 1998; Romano and Santini, 2002; Kirkham, 2005; Ladson *et al.*, 2006). However, field measurements in each soil-vegetation-geology unit of a watershed would take too much effort and expense even under the best of conditions with stone-free soils and shallow rooting depths. In addition, field measurements in areas where rooting depths exceed 2-3 m or where shallow soils are underlain by fractured bedrock are nearly impossible and certainly cannot be completed on a regional scale. The challenge of cost-effective regional TAW mapping can only be met by using remote sensing. Based on our experience with regional mapping of ET and root zone soil moisture in the southwestern U.S. (Fleming *et al.*, 2005; Hendrickx and Hong, 2005; Hong, 2008; Hong *et al.*, 2009, 2011b), Illinois (Hendrickx *et al.*, 2009), Panama (Hendrickx *et al.*, 2005), West Africa (Compaoré *et al.*, 2008), Afghanistan (Hendrickx *et al.*, 2011b), and — more recently — in the Sacramento Mountains of New Mexico and the San Gabriel Mountains of California (Hendrickx *et al.*, 2011a), we recognize that reliable TAW estimates can be derived from a series of Landsat images captured during seasons of water-limited conditions using the following procedure.

Step 1: Select Landsat Images. The availability and quality of Landsat images for any area of interest in the U.S. can be quickly determined at the USGS web page glovis.usgs.gov. After making an inventory of all cloud-free images for the San Gabriel Mountains, we applied two more selection criteria: (1) the image must reflect land surface conditions during the growing season when vegetation is active; and (2) the image must reflect land surface conditions with dry canopies and soil surfaces, i.e., no precipitation in the days before image acquisition. The first criterion assures that the effects of root water uptake are taken into account for determination of TAW in a pixel. The second criterion is needed as we need only information that reflects water uptake from the root zone or evaporation where soils are bare. Therefore, we want to eliminate images that will result in METRIC ET images that include the effects of evaporation from canopy and/or soil surface due to recent precipitation. For this study, we used 15 Landsat images acquired during the growing season in a wet (2005), normal (2003), and dry (2007) precipitation year.

Step 2: Use METRIC and the Evaporative Fraction Method for Retrieval of Soil Moisture Maps. Each Landsat image was processed with METRIC for derivation of the components of the energy balance for each pixel. Equations (2) and (3) were then used to generate the root zone soil moisture map; soil moisture on this map is expressed as the "degree of

soil moisture" from 0 for dry conditions to 1 for conditions where soil moisture is not limiting ET.

Step 3: Determine the Wetness Score for Each Pixel. The wetness score of a pixel is the sum of its "degree of soil moisture" values for all soil moisture maps prepared for a project. If 15 Landsat images are used for the determination of TAW, the wetness score of a pixel may vary from 0 to $15 \times 1.0 = 15.0$. Thus, the wetness score is a relative measure of the overall wetness of a pixel compared to other pixels. As the METRIC algorithm and the evaporative fraction method for soil moisture have a sound scientific basis and have been validated by field measurements and observations, the wetness score map provides a reliable presentation of the overall wetness distribution in the San Gabriel Mountains. As the DPWM cell size is 270×270 m, the 30×30 m Landsat wetness scores have been up-scaled by averaging 81 Landsat scores for each DPWM cell.

Step 4: Determine the Qualitative Relationship between Wetness Score and Total Available Water (TAW). There is ample practical and theoretical evidence that the response of root zone soil moisture to precipitation and ET is, to a large extent, determined by TAW. Following an example by Ritchie (1981b), consider a crop canopy fully covering the ground growing in three soils I, II, and III having a TAW of 10, 120, and 300 mm, respectively. Before the onset of a 30-day period without any precipitation a net precipitation surplus of 300 mm was received that filled the three soils to their maximum TAW. In soils I and II only 10 and 120 mm, respectively, can be stored with the remainder of the surplus precipitation becoming runoff or deep percolation. Assume an ET rate of 5 mm/day and an onset of water stress when more than 50% of the extractable soil water is consumed. Then, these three soils will not show any stress for, respectively, 1, 12, and 30 days. In other words, the amount of available water in these three soils during the dry period is determined only by TAW: the larger the TAW, the higher the degree of soil moisture in the root zone and ET during the dry period. This empirical finding by Ritchie (1981b) has been confirmed by more complete studies using advanced stochastic bucket-type water balance models (Milly, 1994, 2001; Milly and Dunne, 1994; Rodriguez-Iturbe *et al.*, 1999; Laio *et al.*, 2001, 2002; Rodriguez-Iturbe and Porporato, 2004; Seneviratne *et al.*, 2006, 2010). Therefore, we conclude that for most practical applications under water-limited conditions a negative correlation exists between the TAW and the number of days with water-stressed vegetation between two precipitation events. In the context of this study, this means "the lower the wetness score, the lower the TAW."

Step 5: Quantify the Relationship between Wetness Score and Total Available Water (TAW). For the TAW parameterization of distributed bucket-type water balance models, we need a quantitative relationship between the wetness score determined from the soil moisture images retrieved by METRIC on days with cloud-free Landsat images and TAW. We quantify and optimize this relationship by minimizing the differences or mean error between METRIC-observed and DPWM-simulated "degree of soil moisture" distributions for seven different TAW distribution scenarios. Each TAW scenario is characterized by its minimum and maximum value. The lowest TAW value is taken as 15 mm thought to occur in a pixel where most of the water is stored in a few bedrock fractures; the highest TAW value is 1,000 mm thought to occur in a deep soil profile covered by trees. TAW scenario I has a constant low value of 15 mm in all pixels while TAW scenarios II through VII have a minimum value of 15 mm and maximum values of, respectively, 100, 200, 300, 400, 600, and 1,000 mm. These TAW values seem reasonable as compared to the values in the *Australia Data Base* published by Ladson *et al.* (2004, 2006) that contains field measured TAW values for 180 locations in Australia with annual precipitation from about 50 to 1,200 mm. The lowest and highest measured TAW values in Australian soils are, respectively, 20 and 690 mm with most values between 40 and 300 mm.

The optimization procedure that we used is based on a linear relationship between the wetness score and the TAW value. For example, in TAW scenario III, the maximum possible TAW value is set equal to 200 mm. Therefore, the maximum wetness score equals 200 mm and the minimum 15 mm. All other wetness scores for scenario III are found by linear interpolation between these two extreme values. Repeating this procedure for the other maximum possible TAW values yielded seven different regional TAW distributions. For each one of these TAW distributions, DPWM simulated deep percolation — the variable of most interest for groundwater recharge studies — for a period of 30 years generating a large number of daily soil moisture distributions. The optimal TAW distribution is the one with the smallest difference between observed soil moisture values (from METRIC) and simulated soil moisture values (by DPWM). Figure 9 shows that the TAW distribution based on a maximum TAW of 200 mm yields the smallest error and, therefore, we used this TAW distribution for the final simulation to determine the 30-year average groundwater recharge rate in the San Gabriel Mountains. The METRIC TAW distribution captures the variability of TAW at the 30 m pixel scale which is much finer than the traditional TAW

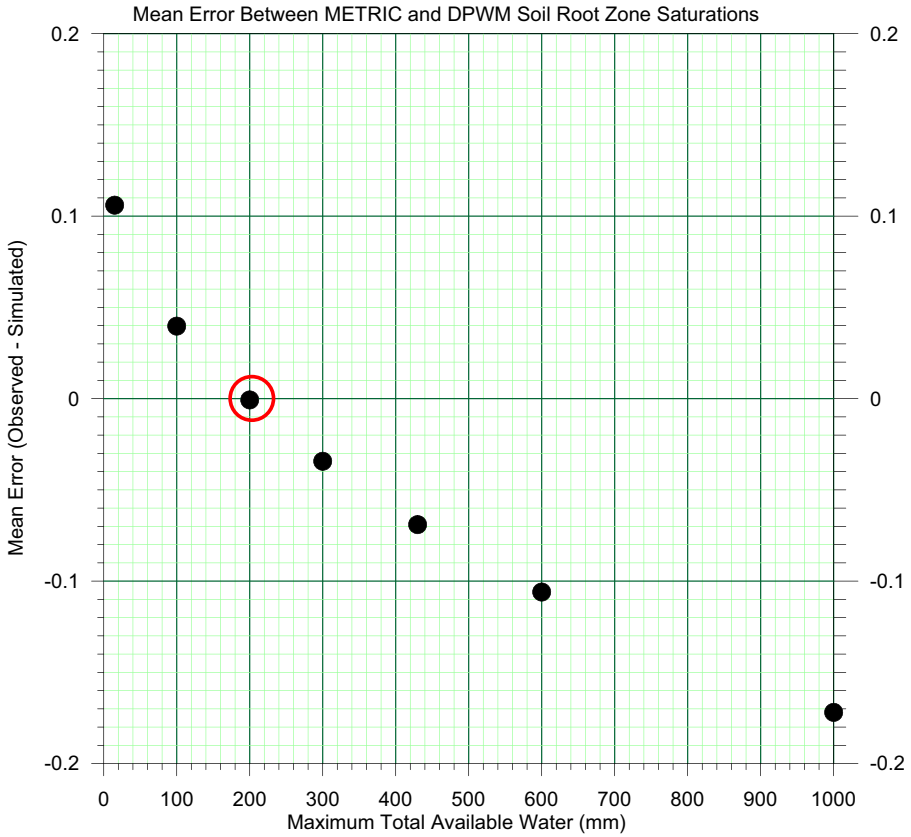

FIGURE 9. Mean Error between METRIC Observed and Distributed Parameter Watershed Model Simulated Root Zone Soil Moisture for Seven Different Total Available Water (TAW) Distributions Based on Their Maximum TAW Value. The TAW distribution with a maximum TAW value of 200 mm yields the smallest error.

distribution that mirrors the soil and vegetation unit scale on the order of 100 m or more.

Benchmark Results for DPWM

Figure 10 shows annual deep percolation, aggregated over the entire San Gabriel Mountain range, simulated with the traditional DPWM approach and with METRIC soil moisture information obtained from Landsat imagery. The average annual recharge for the traditional and METRIC DPWM implementations over the San Gabriel Mountains are, respectively, 0.532 and 0.380 cubic kilometer or 21.3 and 15.2 mm equivalent water depth. So, the use of Landsat imagery for parameterization of the TAW distribution resulted in a lower average annual recharge rate than the one estimated by the traditional DPWM approach. The reason is that Landsat imagery provides the tools to take into account the part of TAW that is stored in bedrock fractures while the traditional DPWM application based on Equation (13) does not. As the recharge rate is negatively correlated with TAW, it decreases when bedrock moisture storage and ET is included in the analysis.

Figure 11 shows the spatial distribution of average annual recharge for the San Gabriel Mountains after parameterizing DPWM with the METRIC-derived optimal TAW distribution (Hendrickx *et al.*, 2011a). The distribution of recharge partly reflects the distribution of the precipitation with higher recharge rates occurring at higher elevations where annual precipitation values increase to 1,400 mm and lower rates at lower elevations where annual precipitation is as low as 250 mm. Such pattern is typical of mountain regions (Guan *et al.*, 2009).

The validation of model-predicted groundwater recharge rates in semiarid regions and mountain blocks is challenging due to the wide range of topographic, geological, geomorphological, and climatic conditions. For that reason, it is recommended to use as many different techniques as possible to constrain estimates of recharge rates including the use of groundwater models (Hendrickx and Walker, 1997; Scanlon, 2004). A simple two-dimensional, cross-sectional groundwater model was developed along cross-section AA′ in the middle of the San Gabriel Mountains as shown in Figure 11. The cross-section runs from Crescenta Valley on the south, follows the Angeles Forest Highway across

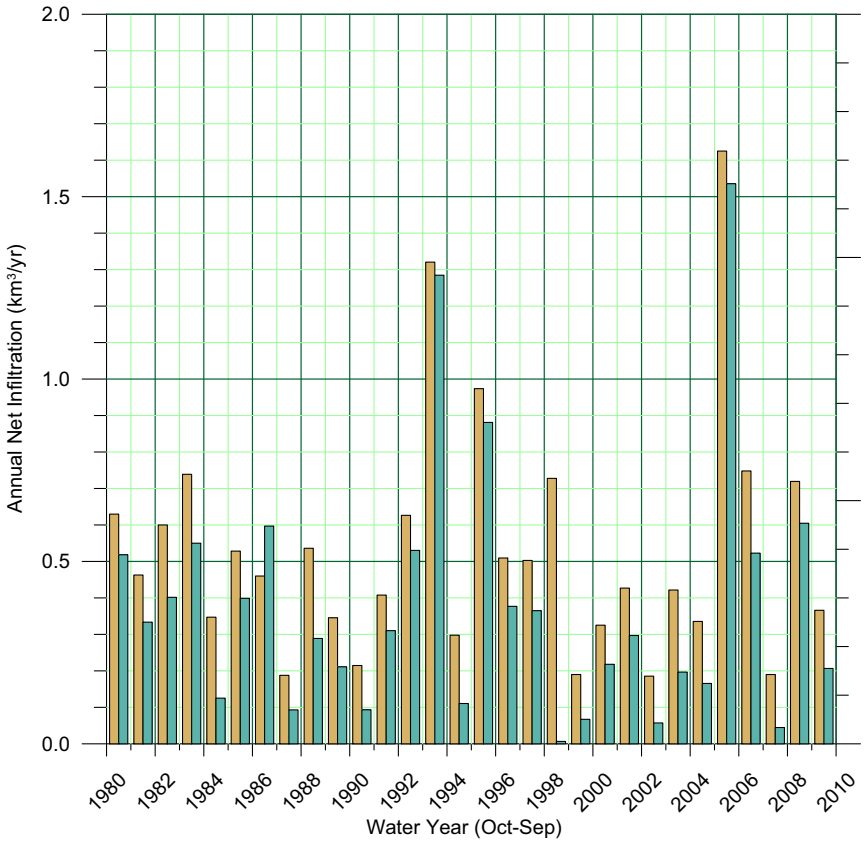

FIGURE 10. Comparison of Average Annual Deep Percolation before (brown) and after (yellow) Using Landsat Imagery for the Parameterization of the Total Available Water (TAW) Distribution in the San Gabriel Mountains.

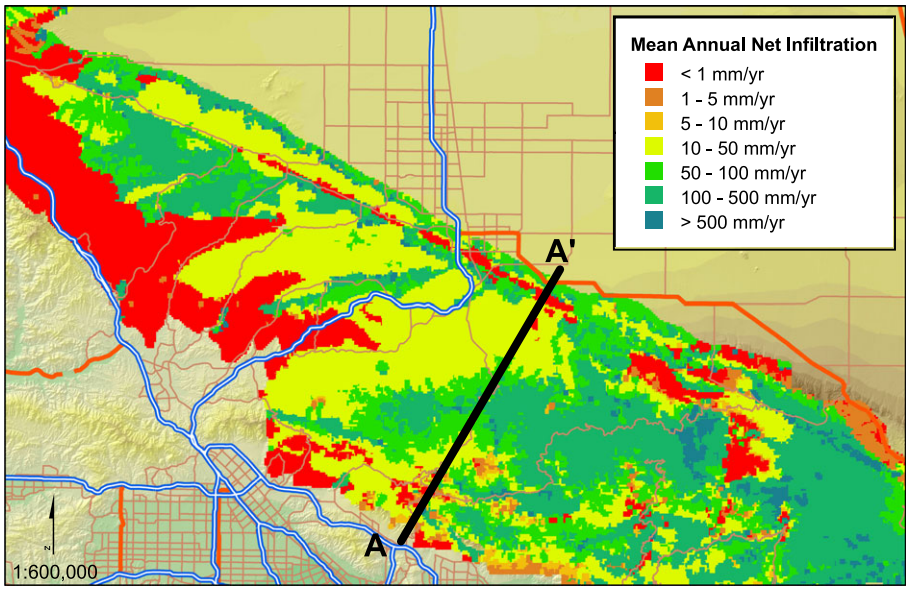

FIGURE 11. Average Annual Groundwater Recharge Rate of Each Pixel Using Landsat Imagery with 30 Years of Daily Simulations of Soil Water Balance with Distributed Parameter Watershed Model (DPWM). The cross-section AA′ was used for the simulation of groundwater table depths before and after using METRIC soil moisture data for calibration of DPWM (see Figure 12).

the crest of the mountain, and terminates at Pearblossom, California on the north. To evaluate the water table elevation within the mountain block, steady-state groundwater simulations were conducted with MODFLOW-SURFACT using spatially distributed annual recharge estimated by DPWM for

the 30-year simulation period. Constant heads were specified on the north and south ends of the cross-section based on the mean groundwater elevations observed in wells in the adjacent valleys. Drain boundary conditions were specified along the cross-section where the cross-section crossed a mapped stream. Hydraulic properties varied in the horizontal direction but were homogeneous in the vertical direction as it was assumed that the geologic unit mapped at the surface represented the underlying units. The vertical hydraulic conductivity used in the groundwater model was the same as assigned to DPWM while the horizontal hydraulic conductivity was assumed to be 10 times the vertical hydraulic conductivity. There are no known wells to provide observations of groundwater elevations along the cross-sections but it is known that streams at the lower elevations, such as Little Rock Creek, have perennial flow from groundwater discharge (Duell, 1987; California Department of Water Resources, 2004), while streams at the higher elevations only have ephemeral flow (Izbicki *et al.*, 2007). Therefore, simulated heads should be high enough to generate discharge at the drain boundary cells at lower elevations, while simulated heads at the higher elevations should be lower than the specified drain elevations. Before DPWM was calibrated with the METRIC soil moisture data, the estimated recharge and corresponding water table appeared too high because permanent discharges were simulated in a high-elevation stream that should be ephemeral. After calibration of DPWM to the METRIC data, the simulated water table corresponded with the observations of perennial and ephemeral stream discharges (Figure 12). This is strong evidence that the use of Landsat imagery can improve the parameterization of TAW distributions and the quality of the groundwater recharge simulations.

Another validation is obtained using detailed soil (Soil Survey Staff, 2013), vegetation (Lennartz *et al.*, 2008), and geology (Ludington *et al.*, 2007) databases. For the San Gabriel Mountains, these data-

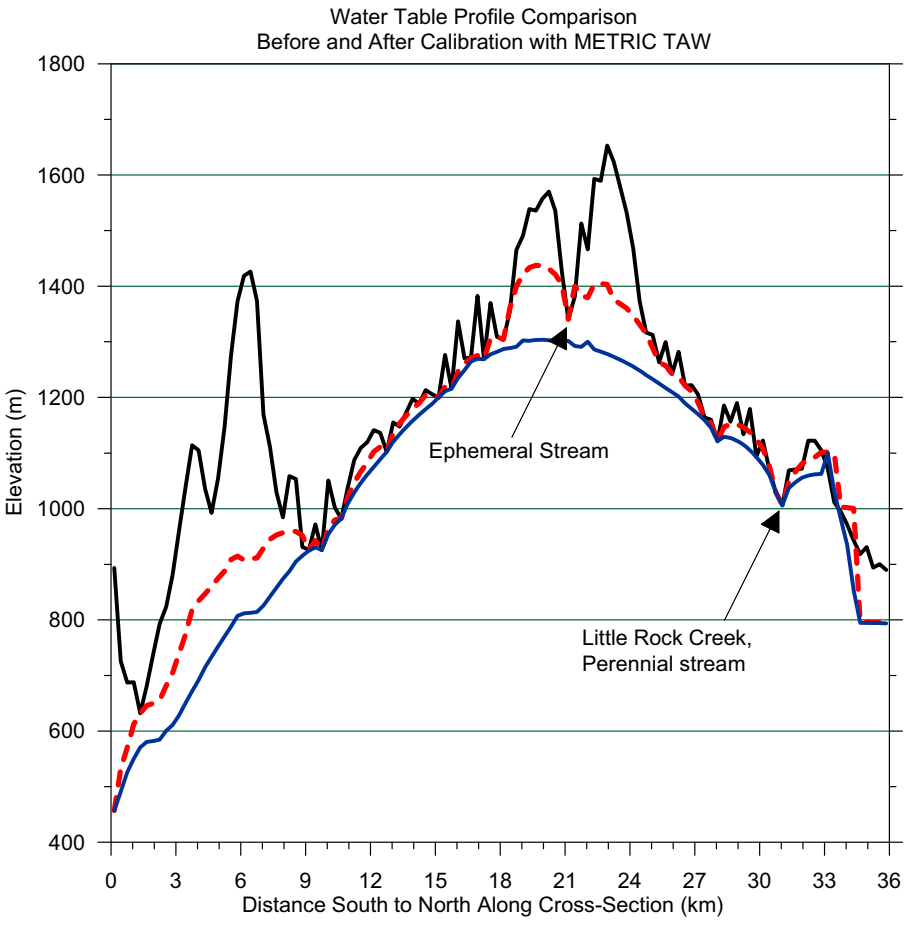

FIGURE 12. Land Surface Elevation and Simulated Groundwater Table Depths without (dashed line) and with (lower solid line) Using Landsat Imagery for the Parameterization of the Total Available Water in Distributed Parameter Watershed Model (DPWM). The ephemeral stream is discharging or perennial when no Landsat imagery is used but becomes clearly ephemeral or nondischarging when Landsat imagery is used for the parameterization of DPWM.

bases contain 229 different soil series, 20 vegetation classes, and 13 bedrock types; together they present $229 \times 20 \times 13 = 59{,}540$ unique environmental units that affect the groundwater recharge processes. For the traditional DPWM approach, the 4,580 soil-vegetation units have been used in Equation (13) for the parameterization of the TAW_{trad} distribution. For the parameterization of the Landsat-based TAW_{METRIC} distribution, no information from these databases was used except the vegetation classes for the assessment of the vegetation height in each cell for estimation of the roughness length needed for calculation of the sensible heat flux. Therefore, TAW_{trad} is a product directly derived from the databases while TAW_{METRIC} has been determined independently from them. Yet, the cited literature above leaves no doubt that TAW principally depends on the soil and vegetation unit. This leads to the hypothesis that the TAW_{METRIC} distribution derived from Landsat imagery should show some relationship with the information in the databases. In other words, if the TAW_{METRIC} distribution is a true representation of total water availability distribution in the San Gabriel Mountains, it should be possible to predict with some degree of accuracy TAW_{METRIC} for each cell in the model from its soil, vegetation, and bedrock geology class. We test this hypothesis by performing a general linear models (GLM) procedure with SAS software; the results of the GLM analysis are presented in Table 5.

Sixty-eight percent of the variability of TAW_{METRIC} in the San Gabriel Mountains is explained by the independent variables Soil, Vegetation, and Bedrock and their interactions S*V, S*B, and V*B with a mean square error of 24 mm. In addition, the values in the table show several other interesting features. First of all, there are two R-squares with a value of 100%; these occur when the independent variables Soil and Vegetation plus their interaction term S*V are part of the linear model for explanation of the variability in the dependent variable TAW_{trad}. The value of 100% is expected as the use of Equation (13) for the calculation of TAW_{trad} only involves Soil and Vegetation characteristics. Of interest is the rather large interaction effect S*V that explains $100 - 62 = 38\%$ of the variability in TAW_{trad}. It means that the effect of Soil on TAW_{trad} depends not only on the soil type but also on the type of Vegetation; the physics for this phenomenon are demonstrated in Equation (13) where in the same soil

TABLE 5. The General Linear Model Procedure of SAS Software Used to Assess How Total Available Water (TAW) Calculated Following the Traditional DPWM Approach (TAW_{trad}) and Using Landsat Imagery (TAW_{METRIC}) Depending on Soil, Vegetation and Bedrock Geology Classes. The dependent variables are TAW_{trad} and TAW_{METRIC}; the independent variables are soil class (S), vegetation class (V) and bedrock geology (B). This analysis was based on the values in 57,423 cells, i.e., the complete population of the area under consideration.

Dependent Variable	Independent Variable[1]	R^2 (%)	Coefficient of Variation (%)	Mean Square Error (mm)	F-value[2] (–)
TAW_{trad}	S, V, B, S*V, S*B, V*B	100	0	0	Infinity
TAW_{METRIC}	S, V, B, S*V, S*B, V*B	68	20	24	56
TAW_{trad}	S, V, B	62	92	78	364
TAW_{METRIC}	S, V, B	60	22	26	336
TAW_{trad}	S, V, S*V	100	0	0	Infinity
TAW_{METRIC}	S, V, S*V	64	21	25	73
TAW_{trad}	S, V	62	92	78	389
TAW_{METRIC}	S, V	60	22	26	346
TAW_{trad}	V, B, V*B	20	133	113	95
TAW_{METRIC}	V, B, V*B	36	28	33	216
TAW_{trad}	V, B	13	139	117	278
TAW_{METRIC}	V, B	34	28	33	952
TAW_{trad}	S, B, S*B	59	96	81	94
TAW_{METRIC}	S, B, S*B	63	21	25	109
TAW_{trad}	S, B	56	99	84	303
TAW_{METRIC}	S, B	58	23	27	327
TAW_{trad}	S	56	100	84	317
TAW_{METRIC}	S	57	23	27	338
TAW_{trad}	V	3	147	124	87
TAW_{METRIC}	V	25	30	36	992
TAW_{trad}	B	11	140	119	562
TAW_{METRIC}	B	16	32	38	941

[1]S = soil unit, V = vegetation unit, and B = bedrock unit. S*V = interaction effect between soil and vegetation, S*B = interaction effect between soil and bedrock, and V*B = interaction effect between vegetation and bedrock. S, V, and B are the main effects while S*V, S*B, and V*B are the interaction effects considered in the general linear models (SAS software).
[2]All F-values have a probability of occurrence <0.0001 indicating that all models are very significant.

different rooting depths will result in different values for TAW_{trad}. The linear model that uses only the independent variable Vegetation to explain the variability in TAW_{trad} yields the smallest R^2 value of 3% but this does not mean that Vegetation is nonsignificant. On the contrary, the S*V interaction effect is a major factor determining TAW_{trad}.

As a check on the GLM analysis, a third TAW distribution was generated consisting of randomly assigned TAW values to each cell of DPWM. The range of these TAW values was identical to the one of TAW_{METRIC}. The R^2 values of the random linear models were all close to zero and never larger than 0.025% indicating that no relationships exist between the independent and dependent variables. In large contrast, the R^2 values of the TAW_{METRIC} linear models ranged from a high of 68 to a low of 16%, although none of the subsurface soil, vegetation, and bedrock information in the databases was used for the generation of TAW_{METRIC}.

We conjecture that the 32% unexplained variability is due to soil, vegetation, and bedrock variability within map units that characterize the heterogeneous San Gabriel mountain block. For example, Bregt and Beemster (1989) found that spatial variability within soil map units caused an error of 50% in the estimation of moisture deficits for soil map scales between 1:25,000 and 1:50,000. Against this background, the explanation of 68% of the variability of TAW_{METRIC} by Soil, Vegetation, Bedrock, and their interactions is a remarkable feat that gives much confidence in the accuracy of the TAW_{METRIC} distribution obtained from Landsat imagery.

Benchmark Conclusion for DPWM

The difference between the average annual groundwater recharges determined without and with optical/thermal satellite imagery is 0.152 cubic kilometer or 6.1 mm. The relative difference between the traditional approach and the METRIC methodology is 28.5%. Therefore, optical/thermal satellite imagery has a large relative impact on the recharge estimates by DPWM. Two validations using the modeled groundwater table elevations along cross-section AA′ and the large percentage of the TAW_{METRIC} distribution explained by soil, vegetation, and bedrock variability provide a strong indication that thermal-equipped Landsat imagery has a great potential to considerably improve groundwater recharge estimates for semiarid mountain blocks.

A recharge difference of only 6.1 mm seems of minor societal importance but it is not. The present price for the water rights of one acre-foot of water in southern California is approximately $10,000. Thus, the monetary value of the recharge difference between the two approaches is well over one billion U.S. dollars and an accurate determination of groundwater recharge is of the utmost importance for fair and equitable settlements of water rights cases.

OVERALL CONCLUSION OF THE THREE CASE STUDIES

In this study, we have benchmarked applications of three operational hydrologic decision support models without and with using optical/thermal satellite imagery for forcing functions, estimation of initial conditions, and model parameterization. The three operational hydrologic decision support tools are the ET Toolbox, the GSSHA model, and the DPWM. Our benchmarking method is straightforward by comparing a typical traditional application of each decision support tool with one that uses information from optical/thermal satellite imagery. Each comparison is based on a performance indicator: annual ET forecasts for ET Toolbox, storm hydrographs for GSSHA, and average annual groundwater recharge volumes for DPWM. Using the SEBAL/METRIC approach for processing MODIS or Landsat imagery, we obtained spatial distributions of the forcing function of ET in ET Toolbox, initial soil moisture conditions in GSSHA, and the model parameter "total available water for transpiration (TAW)" in DPWM.

In the ET Toolbox benchmark test, the annual ET difference between ET computed from a traditional, assigned K_c ET_{ref} ($ET_{Kc\text{-}NMSU}$) and ET computed from K_c derived spatially from METRIC Landsat ($ET_{Kc\text{-}METRIC}$) over the MRGCD command area (i.e., between the traditional and satellite imagery approaches) was 228 mm or 30%; $ET_{Kc\text{-}METRIC}$ was the largest with 771 mm/yr. Considering the validated METRIC applications with MODIS imagery in the Rio Grande Valley, optical/thermal imagery has the potential to considerably improve not only the accuracy of the area-wide ET forecasts in the MRGCD but to also provide detailed information on when, where, and how much water evaporates and transpires. Such information is needed for the development of climate-proofing strategies (Kabat *et al.*, 2005) for the Middle Rio Grande Valley.

In the GSSHA benchmark test, the comparison of two measured hydrographs with the hydrographs simulated with and without using an initial soil moisture distribution generated from Landsat imagery established that the use of Landsat-generated initial soil moisture distributions resulted in superior simulations. In addition, we found that the rank order

stability of soil moisture patterns can make it possible to use SEBAL/METRIC-derived soil moisture maps for model initialization on dates that are days or weeks apart in the future or past from the image day.

In the DPWM benchmark test, the difference between the average annual groundwater recharge determined without and with using a TAW parameterization generated from Landsat imagery equaled 0.152 cubic kilometer or 6.1 mm of water. The relative difference between the traditional approach and the METRIC methodology is a decrease of 28.5% using the latter. Two independent validations based on the groundwater table elevations along a cross-section through the San Gabriel Mountains and the large percentage of the TAW_{METRIC} distribution explained by soil, vegetation, and bedrock variability provide a strong indication that Landsat imagery has a great potential to considerably improve groundwater recharge estimates for semiarid mountain blocks.

The overall conclusion of this benchmark study is that the use of NASA optical/thermal satellite imagery can considerably improve hydrologic decision support tools compared to their traditional implementations. As the water resources of the U.S. are a $200 billion per year economic engine that supports hundreds of thousands of jobs, the costs for Landsat (estimated at about $250 million per year) (Western States Water Council, 2012) and MODIS are only a fraction of the potential benefits. Therefore, this benchmark study demonstrates that the benefits of improved decisions by hydrologic support systems using optical/thermal satellite imagery vastly exceed the costs for acquisition and use of such images.

ACKNOWLEDGMENTS

We acknowledge financial support by NASA under Cooperative Agreement #NNA06CN01A, support by the Idaho Agricultural Experiment Station, and support by the USGS Landsat Science Team (Allen).

LITERATURE CITED

Ahmad, M.-u.-D. and W.G.M. Bastiaanssen, 2003. Retrieving Soil Moisture Storage in the Unsaturated Zone Using Satellite Imagery and Bi-Annual Phreatic Surface Fluctuations. Irrigation and Drainage Systems 17(3):141-161, DOI: 10.1023/A:1025101217521.

Allen, M.F., 2006. Water Dynamics of Mycorrhizas in Arid Soils. *In*: Fungi in Biogeochemical Cycles, G.M. Gadd (Editor). Cambridge University Press, British Mycological Society, Cambridge, United Kingdom, pp. 74-97.

Allen, R., 2011. Skin Layer Evaporation to Account for Small Precipitation Events—An Enhancement to the FAO-56 Evaporation Model. Agricultural Water Management 99(1):8-18.

Allen, R.G., 1997. A Self-Calibrating Method for Estimating Solar Radiation from Air Temperature. Journal of Hydrologic Engineering 2(2):56-67.

Allen, R.G., 2000. Using the FAO-56 Dual Crop Coefficient Method over an Irrigated Region as Part of an Evapotranspiration Intercomparison Study. Journal of Hydrology 229:27-41.

Allen, R.G., 2001. REF-ET: Reference Evapotranspiration Calculation Software for FAO and ASCE Standardized Equations. University of Idaho, Kimberly, Idaho, 82 pp.

Allen, R.G., B. Burnett, W. Kramber, J. Huntington, J. Kjaersgaard, A. Kilic, C. Kelly, and R. Trezza, 2013. Automated Calibration of the METRIC-Landsat Evapotranspiration Process. Journal of the American Water Resources Association 49(3):563-576.

Allen, R.G., A.J. Clemmens, C.M. Burt, K. Solomon, and T. O'Halloran, 2005a. Prediction Accuracy for Projectwide Evapotranspiration Using Crop Coefficients and Reference Evapotranspiration. Journal of Irrigation and Drainage Engineering 131(1):24-36.

Allen, R.G., A. Irmak, R. Trezza, J.M.H. Hendrickx, W.G.M. Bastiaanssen, and J. Kjaersgaard, 2011. Satellite-Based ET Estimation in Agriculture Using SEBAL and METRIC. Hydrologic Processes 25:4011-4027.

Allen, R.G., L.S. Pereira, D. Raes, and M. Smith, 1998. Crop Evapotranspiration: Guidelines for Computing Crop Requirements. Irrigation and Drainage Paper No. 56. Food and Agricultural Organization of the United Nations, Rome, Italy, 300 pp.

Allen, R.G., L.S. Pereira, M. Smith, D. Raes, and J.L. Wright, 2005c. FAO-56 Dual Crop Coefficient Method for Estimating Evaporation from Soil and Application Extensions. Journal of Irrigation and Drainage Engineering 131(1):2-13.

Allen, R.G., W.O. Pruitt, D. Raes, M. Smith, and L.S. Pereira, 2005b. Estimating Evaporation from Bare Soil and the Crop Coefficient for the Initial Period Using Common Soils Information. Journal of Irrigation and Drainage Engineering 131(1):14-23.

Allen, R.G., M. Tasumi, A. Morse, R. Trezza, W. Kramber, and I. Lorite, 2007b. Satellite-Based Energy Balance for Mapping Evapotranspiration with Internalized Calibration (METRIC) - Applications. Journal of Irrigation and Drainage Engineering 133:395-406.

Allen, R.G., M. Tasumi, C.W. Robison, R. Trezza, M. Garcia, A. Brower, D. Toll, and K. Arsenault, 2008a. Exploration of ET Coefficients Derived Using MODIS Satellite-Based METRIC ETrF Versus Awards/ET-Toolbox Based ET Coefficients within the Middle Rio Grande Valley. Miscellaneous Report. University of Idaho, Kimberly Research and Extension Center, Kimberly, Idaho, 116 pp.

Allen, R.G., M. Tasumi, and R. Trezza, 2007a. Satellite-Based Energy Balance for Mapping Evapotranspiration with Internalized Calibration (METRIC) - Model. Journal of Irrigation and Drainage Engineering 133:380-394.

Allen, R.G., M. Tasumi, R. Trezza, C.W. Robison, M. Garcia, D. Toll, K. Arsenault, J.M.H. Hendrickx, and J. Kjaersgaard, 2008b. Comparison of Evapotranspiration Images Derived from MODIS and Landsat along the Middle Rio Grande. ASCE-EWRI Conference, DOI: 10.1061/40976(40316)40987.

Allen, R.G., I.A. Walter, R.L. Elliott, T.A. Howell, D. Itenfisu, M.E. Jensen, and R.L. Snyder, 2005d. The ASCE Standardized Reference Evapotranspiration Equation. American Society of Civil Engineers, Reston, Virginia, 59 pp. with six appendices.

Alley, W.M., 1984. On the Treatment of Evapotranspiration, Soil Moisture Accounting, and Aquifer Recharge in Monthly Water Balance Models. Water Resources Research 20(8):1137-1149.

Anderson, M.C., J.M. Normal, W.P. Kustas, F. Li, J.H. Prueger, and J.R. Mecikalski, 2007. A Climatological Study of Evapotranspiration and Moisture Stress across the Continental United

States: 1. Model Formulation. Journal of Geophysical Research 112:D11112, DOI: 10.1029/12006JD007507.

Asner, G.P., 2001. Cloud Cover in Landsat Observations of the Brazilian Amazon. International Journal of Remote Sensing 22 (18):3855-3862.

Bastiaanssen, W.G.M., 2000. SEBAL-Based Sensible and Latent Heat Fluxes in the Irrigated Gediz Basin, Turkey. Journal of Hydrology 229:87-100.

Bastiaanssen, W.G.M., M.-D. Ahmad, and Y. Chemin, 2002. Satellite Surveillance of Evaporative Depletion across the Indus Basin. Water Resources Research 38(12):1273, DOI: 10.1029/2001WR000386.

Bastiaanssen, W.G.M., M. Menenti, R.A. Feddes, and A.A.M. Holtslag, 1998a. A Remote Sensing Surface Energy Balance Algorithm for Land (SEBAL): Part 1. Formulation. Journal of Hydrology 212-213:198-212.

Bastiaanssen, W.G.M., D.J. Molden, and I.W. Makin, 2000. Remote Sensing for Irrigated Agriculture: Examples from Research and Possible Applications. Agricultural Water Management 46 (2):137-155.

Bastiaanssen, W.G.M., E.J.M. Noordman, H. Pelgrum, G. Davids, B.P. Thoreson, and R.G. Allen, 2005. SEBAL Model with Remotely Sensed Data to Improve Water-Resources Management under Actual Field Conditions. Journal of Irrigation and Drainage Engineering, ASCE, 131(1):85-93.

Bastiaanssen, W.G.M., H. Pelgrum, P. Droogers, H.A.R. de Bruin, and M. Menenti, 1997. Area-Averaged Estimates of Evaporation, Wetness Indicators and Top Soil Moisture During Two Golden Days in EFEDA. Agricultural and Forest Meteorology 87(2-3):119-137.

Bastiaanssen, W.G.M., H. Pelgrum, J. Wang, Y. Ma, J.F. Moreno, G.J. Roerink, and T. van der Wal, 1998b. A Remote Sensing Surface Energy Balance Algorithm for Land (SEBAL): Part 2: Validation. Journal of Hydrology 212-213:213-229.

Belmans, J.G., J. Wesseling, and R.A. Feddes, 1983. Simulation of the Water Balance of a Cropped Soil, SWATRE. Journal of Hydrology 63:271-286.

Bexfield, L.M. and S.K. Anderholm, 1997. Water-Quality Assessment of the Rio Grande Valley, Colorado, New Mexico, Texas—Ground-Water Quality in the Rio Grande Flood Plain, Cochiti Lake, New Mexico, to El Paso, Texas, 1995. Water-Resources Investigations Report 96-4249. U.S. Geological Survey, Albuquerque, New Mexico, 93 pp.

Bolle, H.-J., J.-C. André, J.L. Arrue, H.K. Barth, P. Bessemoulin, A. Brasa, H.A.R. de Bruin, G. Dugdale, E.T. Engman, D.L. Vans, R. Fantechi, F. Fiedler, A. de van Griend, A.C. Imenson, A. Jochum, P. Kabat, T. Kratzsch, J.-P. Lagouarde, I. Langer, R. Llamas, E. Lopez-Baeza, J. Melia Miralles, L.S. Muniosguren, F. Nerr, J. Noilhan, H.R. Oliver, R. Roth, J. Sanchez Diaz, M. de Santa Olalla, W.J. Shuttleworth, H. Soergaard, H. Stricker, J. Thornes, M. Vauclin, and D. Wickland, 1993. EFEDA: European Field Experiment in a Desertification-Threatened Area. Annales Geophysicae 11:173-189.

Boni, G., D. Entekhabi, and F. Castelli, 2001. Land Data Assimilation with Satellite Measurements for the Estimation of Surface Energy Balance Components and Surface Control on Evaporation. Water Resources Research 37(6):1713-1722.

Bornyasz, M.A., R.C. Graham, and M.F. Allen, 2005. Ectomycorrhizae in a Soil-Weathered Granitic Bedrock Regolith: Linking Matrix Resources to Plants. Geoderma 126:141-160.

Bouma, J. and P. Droogers, 1999. Comparing Different Methods for Estimating the Soil Moisture Supply Capacity of a Soil Series Subjected to Different Types of Management. Geoderma 92:185-197.

Bregt, A.K. and J.G.R. Beemster, 1989. Accuracy in Predicting Moisture Deficits and Changes in Yield from Soil Maps. Geoderma 43:301-310.

Brower, A., 2008. ET Toolbox Evapotranspiration Toolbox for the Middle Rio Grande, A Water Resources Decision Support Tool. Report, Water Resources Division, Technical Service Center, Bureau of Reclamation, US Department of the Interior, Denver, Colorado, 167 pp.

Brutsaert, W. and M. Sugita, 1992. Application of Self-Preservation in the Diurnal Evolution of the Surface Energy Budget to Determine Daily Evaporation. Journal of Geophysical Research 97: D17, 18377-18382.

Byrd, A.R., 2013. Surface Water and Groundwater Effects of Land Use Change in the Kishwaukee, IL Watershed. Technical Report.

California Department of Water Resources, 2004. South Lahontan Hydrologic Region. Antelope Valley Groundwater Basin. California's Groundwater Bulletin 118.

Cassel, D.K. and D.R. Nielsen, 1986. Field Capacity and Available Water Capacity. *In*: Methods of Soil Analysis, Part I. Agronomy Monograph Series No. 9 (Second Edition), A. Klute (Editor). Soil Science Society of America, Madison, Wisconsin, pp. 901-926.

Compaoré, H., J.M.H. Hendrickx, S.-H. Hong, J. Friesen, N.C. van de Giesen, C. Rodgers, J. Szarzynski, and P.L.G. Vlek, 2008. Evaporation Mapping at Two Scales Using Optical Imagery in the White Volta Basin, Upper East Ghana. Physics and Chemistry of the Earth, Parts A/B/C 33:127-140, DOI: 10.1016/j.pce.2007.1004.1021.

Crago, R.D., 1996. Comparison of the Evaporative Fraction and the Priestley-Taylor α for Parameterizing Daytime Evaporation. Water Resources Research 32:1403-1409.

Daniel B. Stephens & Associates, Inc., 2008. Mean Annual Recharge for the Tule Desert Hydrographic Basin, Lincoln County, Nevada. Prepared for Lincoln County Water District and Vidler Water Company. Report, Daniel B. Stephens & Associates, Inc., Albuquerque, New Mexico, 231 pp.

Daniel B. Stephens & Associates, Inc., 2010a. Draft - Manual for the Distributed Parameter Watershed Model (DPWM). Report, Daniel B. Stephens & Associates, Inc., Albuquerque, New Mexico, 83 pp.

Daniel B. Stephens & Associates, Inc., 2010b. Water Master Plan. Prepared for Big Bear City Community Services District, Big Bear City CA. Report, Daniel B. Stephens & Associates, Inc., Albuquerque, New Mexico, 464 pp.

Daniel B. Stephens & Associates, Inc., 2011. Revised Groundwater Flow Model and Predictive Simulation Results Coso Operating Company Hay Ranch Water Extraction and Delivery System Conditional Use Permit (CUP 2007-003). Prepared for County of Inyo CA. Report, Daniel B. Stephens & Associates, Inc., Albuquerque, New Mexico.

Davies, J.A. and C.D. Allen, 1973. Equilibrium, Potential and Actual Evapotranspiration from Cropped Surfaces in Southern Ontario. Journal of Applied Meteorology 12:649-657.

De Bruin, H.A.R., 1983. A Model for the Priestley-Taylor Parameter Alpha. Journal of Climate and Applied Meteorology 22:572-578.

Downer, C.W. and F.L. Ogden, 2004. GSSHA: A Model for Simulating Diverse Streamflow Generating Processes. Journal of Hydrologic Engineering 9:161-174.

Downer, C.W. and F.L. Ogden, 2006. Gridded Surface Subsurface Hydrologic Analysis (GSSHA) User's Manual; Version 1.43 for Watershed Modeling System 6.1. ERDC/CHL SR-06-1. Report, U.S. Army Corps of Engineers.

Duell, L.F.W., 1987. Geohydrology of the Antelope Valley Area, California, and Design for a Ground-Water-Quality Monitoring Network. U.S. Geological Survey, Water-Resources Investigations Report 84-4081, 76 pp.

Engle, E.M., J.B.J. Harrison, J.M.H. Hendrickx, and B. Borchers, 2010. Digital Soil Boundary Detection Using Quantitative Hydrologic Remote Sensing. *In*: Digital Soil Map-

ping: Bridging Research, Environmental Application, and Operation, J.L. Boettinger, D.W. Howell, A.C. Moore, A.E. Hartemink, and S. Kienast-Brown (Editors). Springer, Dordrecht, pp. 123-134.

Engle, E.M., J.B.J. Harrison, J.M.H. Hendrickx, and B. Borchers, 2014. Remote Sensing for Soil Map Unit Boundary Detection. *In*: Military Geosciences in the 21st Century. Reviews in Engineering Geology Series, R.S. Harmon and E.V. MacDonald (Editors). Geological Society of America, Boulder, Colorado, pp. 119-130.

Feddes, R.A., H. Hoff, M. Bruen, T. Dawson, P. de Rosnay, P. Dirmeyer, R.B. Jackson, P. Kabat, A. Kleidon, A. Lilly, and A.J. Pitman, 2001. Modeling Root Water Uptake in Hydrological and Climate Models. Bulletin of the American Meteorological Society 82(12):2797-2809.

Feddes, R.A., P. Kabat, P.J.T.V. Bakel, J.J.B. Bronswijk, and J. Halbertsma, 1988. Modelling Soil Water Dynamics in the Unsaturated Zone - State of the Art. Journal of Hydrology 100:69-111.

Feddes, R.A., P.J. Kowalik, and H. Zaradny, 1978. Simulation of Field Water Use and Crop Yield. Pudoc, Wageningen, The Netherlands.

Fleming, K., J.M.H. Hendrickx, and S.-H. Hong, 2005. Regional Mapping of Root Zone Soil Moisture Using Optical Satellite Imagery. Proceedings of International Society for Optical Engineering, SPIE 5811:159-170.

Flint, A. and L. Flint, 2007. Application of the Basin Characterization Model to Estimate In-Place Recharge and Runoff Potential in the Basin and Range Carbonate-Rock Aquifer System, White Pine County, Nevada, and Adjacent Areas in Nevada and Utah. USGS Scientific Investigations Report 2007-5099. USGS, Reston, Virginia, 20 pp.

Fry, J., G. Xian, S. Jin, J. Dewitz, C. Homer, L. Yang, C. Barnes, N. Herold, and J. Wickham, 2011. Completion of the 2006 National Land Cover Database for the Conterminous United States. PE&RS 77(9):858-864.

Guan, H., J.L. Wilson, and H. Xie, 2009. A Cluster-Optimizing Regression-Based Approach for Precipitation Spatial Downscaling in Mountainous Terrain. Journal of Hydrology 375(3-4):578-588.

Guswa, A.J., M.A. Celia, and I. Rodriguez-Iturbe, 2002. Models of Soil Moisture Dynamics in Ecohydrology: A Comparative Study. Water Resources Research 38(9):1166, DOI: 10.1029/2001WR000826.

Hafeez, M., M. Andreini, J. Liebe, J. Friesen, A. Marx, and N.v.d. Giesen, 2006. Hydrological Parameterization Through Remote Sensing in Volta Basin, West Africa. International Journal of River Basin Management 4(4):1-8.

Hain, C.R., W.T. Crow, J.R. Mecikalski, M.C. Anderson, and T. Holmes, 2011. An Intercomparison of Available Soil Moisture Estimates from Thermal Infrared and Passive Microwave Remote Sensing and Land Surface Modeling. Journal of Geophysical Research 116(D15):D15107.

Hain, C.R., J.R. Mecikalski, and M.C. Anderson, 2009. Retrieval of an Available Water-Based Soil Moisture Proxy from Thermal Infrared Remote Sensing. Part I: Methodology and Validation. Journal of Hydrometeorology 10:665-683, DOI: 10.1175/2008JHM1024.1171.

Hendrickx, J.M.H., W.G.M. Bastiaanssen, E.J.M. Noordman, S.-H. Hong, and L.E. Calvo Gobbeti, 2005. Estimation of Regional Actual Evapotranspiration in the Panama Canal Watershed. *In*: The Rio Chagres: A Multidisciplinary Profile of a Tropical Watershed, R.S. Harmon (Editor). Springer, Dordrecht, The Netherlands, pp. 315-324.

Hendrickx, J.M.H., J.B.J. Harrison, B. Borchers, J.R. Kelley, S. Howington, and J. Ballard, 2011b. High-Resolution Soil Moisture Mapping in Afghanistan, Proceedings of International Society for Optical Engineering, SPIE, 8017, 801710, DOI: 10.1117/801712.887255.

Hendrickx, J.M.H. and S.-H. Hong, 2005. Mapping Sensible and Latent Heat Fluxes in Arid Areas Using Optical Imagery. Proceedings of International Society for Optical Engineering, SPIE 5811:138-146.

Hendrickx, J.M.H., F.M. Phillips, and J.B.J. Harrison, 2003. Water Flow Processes in Arid and Semi-Arid Vadose Zones. *In*: Understanding Water in a Dry Environment. Hydrological Processes in Arid and Semi-Arid Zones, I. Simmers (Editor). A.A. Balkema Publishers, Lisse, The Netherlands, pp. 151-210.

Hendrickx, J.M.H., N.R. Pradhan, S.-H. Hong, F.L. Ogden, A.R. Byrd, and D. Toll, 2009. Improvement of Hydrologic Model Soil Moisture Predictions Using SEBAL Evapotranspiration Estimates. Proceedings of International Society for Optical Engineering, SPIE 7303:730311.

Hendrickx, J.M.H., T.G. Umstot, and J.L. Wilson, 2011a. Ground Water Recharge in Semi-Arid Mountain Blocks: San Gabriel Mountains Case Study. Abstract at Soil Science Society of America International Annual Meeting, October 16-19, San Antonio, Texas, p. 116.

Hendrickx, J.M.H. and G. Walker, 1997. Recharge from Precipitation. *In*: Recharge of Phreatic Aquifers in (Semi)-Arid Areas, I. Simmers (Editor). Balkema, Rotterdam, The Netherlands, pp. 19-114.

Hendrickx, J.M.H., P.J. Wierenga, and M.S. Nash, 1990. Variability of Soil Water Tension and Soil Water Content. Agricultural Water Management 18:135-148.

Hendrickx, J.M.H., P.J. Wierenga, M.S. Nash, and D.R. Nielsen, 1986. Boundary Location from Texture, Soil Moisture, and Infiltration Data. Soil Science Society of America Journal 50:1515-1520.

Hillel, D., 1998. Environmental Soil Physics. Academic Press, San Diego, California, 771 pp.

Hong, S.-H., 2008. Mapping Regional Distributions of Energy Balance Components Using Optical Remotely Sensed Imagery. Ph.D. Dissertation, 378 pp., New Mexico Institute of Mining and Technology, Socorro, New Mexico.

Hong, S.-H., J.M.H. Hendrickx, and B. Borchers, 2005. Effect of Scaling Transfer between Evapotranspiration Maps Derived from LandSat 7 and MODIS Images. Proceedings of International Society for Optical Engineering, SPIE 5811:147-158.

Hong, S.-H., J.M.H. Hendrickx, and B. Borchers, 2009. Up-Scaling of SEBAL Derived Evapotranspiration Maps from Landsat (30 m) to MODIS (250 m) Scale. Journal of Hydrology 370:122-138, DOI: 10.1016/j.jhydrol.2009.1003.1002.

Hong, S.-H., J.M.H. Hendrickx, and B. Borchers, 2011a. Down-Scaling of SEBAL Derived Evapotranspiration Maps from MODIS (250 m) to Landsat (30 m) Scales. International Journal of Remote Sensing 32(21):6457-6477.

Hong, S.-H., J.M.H. Hendrickx, and B. Borchers, 2011b. Down-Scaling of SEBAL Derived Evapotranspiration Maps from MODIS (250 m) to Landsat (30 m) Scales. International Journal of Remote Sensing 32:1-21.

Hupet, F., M.C.T. Trought, M. Greven, S.R. Green, and B.E. Clothier, 2005. Data Requirements for Identifying Macroscopic Water Stress Parameters: A Study on Grapevines. Water Resources Research 41(6):W06008.

Hyndman, D.W., A.D. Kendall, and N.R.H. Welty, 2007. Evaluating Temporal and Spatial Variations in Recharge and Streamflow Using the Integrated Landscape Hydrology Model (ILHM). *In*: Subsurface Hydrology: Data Integration for Properties and Processes, D.W. Hyndman, F.D. Day-Lewis, and K. Singha (Editors). Geophysical Monograph Series 171, American Geophysical Union, Washington, D.C., pp. 121-141.

Irmak, A., R. Allen, J. Kjaersgaard, J. Huntington, B. Kamble, R. Trezza, and I. Ratcliffe, 2012. Operational Remote Sensing of ET and Challenges. *In*: Evapotranspiration – Remote Sensing and Modeling, A. Irmak (Editor). InTech, pp. 467-492.

Irmak, A., I. Ratcliffe, P. Ranade, K. Hubbard, R.K. Singh, B. Kamble, and J. Kjaersgaard, 2011. Estimation of Land Surface Evapotranspiration with a Satellite Remote Sensing Procedure. Great Plains Research 21:73-88.

Irmak, S., A. Irmak, T.A. Howell, D.L. Martin, J.O. Payero, and K.S. Copeland, 2008. Variability Analyses of Alfalfa-Reference to Grass-Reference Evapotranspiration Ratios in Growing and Dormant Seasons. Journal of Irrigation and Drainage Engineering 134(2):147-159.

Israelsen, O.W. and F.L. West, 1922. Bulletin No. 183 - Water Holding Capacity of Irrigated Soils. Utah State Agricultural Experiment Station Bulletins. Paper 149, pp. 1-24. http://digitalcommons.usu.edu/uaes_bulletins/149 pp, *accessed* October 2015.

Izbicki, J.A., R.U. Johnson, J. Kulongoski, and S. Predmore, 2007. Ground-Water Recharge from Small Intermittent Streams in the Western Mojave Desert, California. *In*: Ground-Water Recharge in the Arid and Semiarid Southwestern United States. Geological Survey Professional Paper, Volume 1703, D.A. Stonestrom, J. Constantz, T.P.A. Ferré, and S.A. Leake (Editors). U.S. Geological Survey, Menlo Park, California, pp. 157-184.

Jackson, R.B., J.S. Sperry, and T.E. Dawson, 2000. Root Water Uptake and Transport: Using Physiological Processes in Global Predictions. Trends in Plant Science 5(11):482-488.

Jacobs, J.M., S.L. Mergelsberg, A.F. Lopera, and D.A. Myers, 2002. Evapotranspiration from a Wet Prairie Wetland under Drought Conditions: Paynes Prairie Preserve, Florida, USA. WETLANDS 22:374-385.

Jensen, M.E., 1998. Coefficients for Vegetative Evapotranspiration and Open Water Evaporation for the Lower Colorado River Accounting System. Report, U.S. Bureau of Reclamation, Boulder City, Nevada.

Jury, W.A. and R.E. Horton, 2004. Soil Physics (Sixth Edition). John Wiley & Sons, Inc., Hoboken, New Jersey, 370 pp.

Kabat, P., W. van Vierssen, J. Veraart, P. Vellinga, and J. Aerts, 2005. Climate Proofing the Netherlands. Nature 438(7066):283-284.

Kachanoski, R.G. and E. de Jong, 1988. Scale Dependence and the Temporal Persistence of Spatial Patterns of Soil Water Storage. Water Resources Research 24(1):85-91.

Karimi, P. and W.G.M. Bastiaanssen, 2015. Spatial Evapotranspiration, Rainfall and Land Use Data in Water Accounting–Part 1: Review of the Accuracy of the Remote Sensing Data. Hydrology and Earth System Sciences 19:507-532.

Kay, R.T. and A. Trugestaad, 1998. Hydrology, Water Quality and Nutrient Loads to the Bauman Park Lake, Cherry Valley, Winnebago County, Illinois, May 1996-April 1997. Water-Resources Investigations Report 98-4087, 65 pp., USGS, Urbana, Illinois.

Kilic, A., J. Huntington, R. Allen, C. Morton, B. Kamble, N. Gorelick, D. Thau, R. Trezza, I. Ratcliffe, and C. Robison, 2014. An Evapotranspiration Mapping Tool at Landsat Resolution on the Google Earth Engine: EEFlux. PECORA-ASPRS Conference Abstract. *In*: PECORA-ASPRS Conference, Denver, Colorado. http://www.asprs.org/a/Pecora19-ISPRS/Abstracts/MTSTC1-146.pdf, *accessed* October 2015.

Kirkham, M.B., 2005. Principles of Soil and Plant Water Relations. Elsevier - Academic Press, New York City, New York, 500 pp.

Kleissl, J., S.-H. Hong, and J.M.H. Hendrickx, 2009. New Mexico Scintillometer Network. Supporting Remote Sensing and Hydrologic and Meteorological Models. Bulletin American Meteorological Society 90(2):207-218, DOI: 10.1175/2008BAMS2480.1171.

Kustas, W.P. and J.M. Norman, 1999. Evaluation of Soil and Vegetation Heat Flux Predictions Using a Simple Two-Source Model with Radiometric Temperatures for Partial Canopy Cover. Agricultural and Forest Meteorology 94:13-29.

Ladson, A., J. Lander, A. Western, and R. Grayson, 2004. Estimating Extractable Soil Moisture Content for Australian Soils. Technical Report 04/3, Cooperative Research Center for Catchment Hydrology, Canberra, Australia, 92 pp.

Ladson, A.R., J.R. Lander, A.W. Western, R.B. Grayson, and L. Zhang, 2006. Estimating Extractable Soil Moisture Content for Australian Soils from Field Measurements. Soil Research 44 (5):531-541.

Laio, F., A. Porporato, C.P. Fernandez-Illescas, and I. Rodriguez-Iturbe, 2001. Plants in Water-Controlled Ecosystems: Active Role in Hydrologic Processes and Response to Water Stress: IV. Discussion of Real Cases, Advances in Water Resources 24 (7):745-762.

Laio, F., A. Porporato, L. Ridolfi, and I. Rodriguez-Iturbe, 2002. On the Seasonal Dynamics of Mean Soil Moisture. Journal of Geophysical Research 107(D15):4272.

Langman, J.B., 2009. Traveltime of the Rio Grande in the Middle Rio Grande Basin, Water Years 2003-05. Scientific Investigations Report 2007-5292, U.S. Geological Survey, 34 pp.

Lennartz, S., T. Bax, J. Aycrigg, A. Davidson, M. Reid, and R. Congalton, 2008. Final Report on Land Cover Mapping Methods for California Map Zones 3, 4, 5, 6, 12, and 13. ftp://ftp.gap.uidaho.edu/products/california/, *accessed* January 2013.

Liu, S., W.D. Graham, and J.M. Jacobs, 2005. Daily Potential Evapotranspiration and Diurnal Climate Forcings: Influence on the Numerical Modelling of Soil Water Dynamics and Evapotranspiration. Journal of Hydrology 309:39-52.

Ludington, S., B.C. Moring, R.J. Miller, P.A. Stone, A.A. Bookstrom, D.R. Bedford, J.G. Evans, G.A. Haxel, C.J. Nutt, K.S. Flyn, and M.J. Hopkins, 2007. Preliminary Integrated Geologic Map Databases for the United States. Western States: California, Nevada, Arizona, Washington, Oregon, Idaho, and Utah. Version 1.3. Updated December 2007. http://pubs.usgs.gov/of/2005/1305/, *accessed* January 2008, 2013.

Manabe, S., 1969. 1. The Atmospheric Circulation and the Hydrology of the Earth's Surface. Monthly Weather Review 97(11):739-774.

Milly, P.C.D., 1994. Climate, Soil Water Storage, and the Average Annual Water Balance. Water Resources Research 30(7):2143-2156.

Milly, P.C.D., 2001. A Minimalist Probabilistic Description of Root Zone Soil Water. Water Resources Research 37(3):457-463.

Milly, P.C.D. and K.A. Dunne, 1994. Sensitivity of the Global Water Cycle to the Water-Holding Capacity of Land. Journal of Climate 7:506-526.

Moayyad, B., S.A. Bawazir, J.P. King, S.-h. Hong, and J.M.H. Hendrickx, 2003. Groundwater Depth and Arid Zone Riparian Evapotranspiration. *In*: Understanding Water in a Dry Environment Hydrological Processes in Arid and Semi-Arid Zones, I. Simmers (Editor). A.A. Balkema Publishers, Lisse, The Netherlands, pp. 188-195.

Mohamed, Y.A., W.G.M. Bastiaanssen, and H.H.G. Savenije, 2004. Spatial Variability of Evaporation and Moisture Storage in the Swamps of the Upper Nile Studied by Remote Sensing Techniques. Journal of Hydrology 289:145-164, DOI: 10.1016/j.jhydrol.2003.1011.1038.

Nelson, J.W., L.C. Holmes, and E.C. Eckmann, 1914. Soil Survey of the Middle Rio Grande Valley Area, New Mexico. United States Department of Agriculture, Washington, D.C., 56 pp.

Nepstad, D.C., C.R. de Carvalho, E.A. Davidson, P.H. Jipp, P.A. Lefebvre, G.H. Negreiros, E.D. da Silva, T.A. Stone, S.E. Trumbore, and S. Vieira, 1994. The Role of Deep Roots in the Hydrological and Carbon Cycles of Amazonian Forests and Pastures. Nature 372(6507):666-669.

Ogden, F.L., H.O. Sharif, S.U.S. Senarath, J.A. Smith, M.L. Baeck, and J.R. Richardson, 2000. Hydrologic Analysis of the Fort Collins, Colorado, Flash Flood of 1997. Journal of Hydrology 228:82-100.

Owe, M. and A.A. van de Griend, 1990. Daily Surface Moisture Model for Large Area Semi-Arid Land Applications with Limited Climate Data. Journal of Hydrology 121:119-132.

Pradhan, N.R., A.R. Byrd, F.L. Ogden, and J.M.H. Hendrickx, 2012. SEBAL Evapotranspiration Estimates for the Improvement of Distributed Hydrologic Model Runoff and Soil Moisture Predictions. *In*: Remote Sensing and Hydrology, C.M.U. Neale and M.H. Cosh (Editors). IAHS, Jackson Hole, Wyoming, pp. 435-439.

Ratliff, L.F., J.T. Ritchie, and D.K. Cassel, 1983. Field-Measured Limits of Soil Water Availability as Related to Laboratory-Measured Properties. Soil Science Society of America Journal 47:770-775.

Rawls, W.J., D.L. Brakensiek, and K.E. Saxton, 1982. Estimation of Soil Water Properties. Transactions of the ASAE 25(5):1316-1320.

Ritchie, J.T., 1981a. Water Dynamics in the Soil-Plant-Atmosphere. Plant and Soil 58:81-96.

Ritchie, J.T., 1981b. Soil Water Availability. Plant and Soil 58 (1):327-338.

Ritchie, J.T., A. Gekakis, and A. Suleiman, 1999. Simple Model to Estimate Field-Measured Soil Water Limit. Transactions of the ASAE 42:1609-1614.

Rodriguez-Iturbe, I. and A. Porporato, 2004. Ecohydrology of Water-Controlled Ecosystems. Cambridge University Press, Cambridge, United Kingdom, 442 pp.

Rodriguez-Iturbe, I., A. Porporato, L. Ridolfi, V. Isham, and D.R. Cox, 1999. Probabilistic Modelling of Water Balance at a Point: The Role of Climate, Soil and Vegetation. Proceedings: Mathematical, Physical and Engineering Sciences 455(1990):3789-3805.

Romano, N. and A. Santini, 2002. Water Retention and Storage. *In*: Methods of Soil Analysis, Part 1, J. Dane and C. Topp (Editors). Soil Science Society of America, Madison, Wisconsin, pp. 721-738.

Sandia National Laboratory, 2007. Simulation of Net Infiltration for Present-Day and Potential Future Climates, Yucca Mountain Project. MDL-NBS-HS-000023 REV 01. May 2007 Report.

Sano, E.E., L.G. Ferreira, G.P. Asner, and E.T. Steinke, 2007. Spatial and Temporal Probabilities of Obtaining Cloud-Free Landsat Images Over the Brazilian Tropical Savanna. International Journal of Remote Sensing 28(12):2739-2752.

Scanlon, B.R., 2004. Evaluation of Methods of Estimating Recharge in Semiarid and Arid Regions in the Southwestern U.S. *In*: Groundwater Recharge in a Desert Environment. The Southwestern United States, J.F. Hogan, F.M. Phillips, and B.R. Scanlon (Editors). American Geophysical Union, Washington, D.C., pp. 235-254.

Schaake, J.C., V.I. Koren, Q.-Y. Duan, K. Mitchell, and F. Chen, 1996. Simple Water Balance Model for Estimating Runoff at Different Spatial and Temporal Scales. Journal of Geophysical Research 101(D3):7461-7475.

Schroeder, P.R., T.S. Dozier, P.A. Zappi, B.M. McEnroe, J.W. Sjostrom, and R.L. Peyton, 1994. The Hydrologic Evaluation of Landfill Performance (HELP) Model: Engineering Documentation for Version 3. U.S. Environmental Protection Agency Office of Research and Development, Washington, D.C., September 1994, EPA/600/R-94/168b.

Schuurmans, J.M., P.A. Troch, A.A. Veldhuizen, W.G.M. Bastiaanssen, and M.F.P. Bierkens, 2003. Assimilation of Remotely Sensed Latent Heat Flux in a Distributed Hydrological Model. Advances in Water Resources 26:151-159.

Scott, C.A., W.G.M. Bastiaanssen, and M.-u.-D. Ahmad, 2003. Mapping Root Zone Soil Moisture Using Remotely Sensed Optical Imagery. Journal of Irrigation and Drainage Engineering 129 (5):326-335.

Sellers, P.J., R.E. Dickinson, D.A. Randall, A. K. Betts, F.G. Hall, J.A. Berry, G.J. Collatz, A.S. Denning, H.A. Mooney, C.A. Nobre, N. Sato, C.B. Field, and A. Henderson-Sellers, 1997. Modeling the Exchanges of Energy, Water, and Carbon Between Continents and the Atmosphere. Science 275(5299):502-509.

Senarath, S.U.S., F.L. Ogden, C.W. Downer, and H.O. Sharif, 2000. On the Calibration and Verification of Distributed, Physically-Based, Continuous, Hortonian Hydrologic Models. Water Resources Research 36(6):1495-1510.

Seneviratne, S.I., T. Corti, E.L. Davin, M. Hirschi, E.B. Jaeger, I. Lehner, B. Orlowsky, and A.J. Teuling, 2010. Investigating Soil Moisture-Climate Interactions in a Changing Climate: A Review. Earth-Science Reviews 99(3/4):125-161.

Seneviratne, S.I., R.D. Koster, Z. Guo, P. Dirmeyer, E. Kowalczyk, and D. Lawrence, 2006. Soil Moisture Memory in AGCM Simulations: Analysis of Global Land–Atmosphere Coupling Experiment (GLACE) Data. Journal of Hydrometeorology 7(5):1090-1112.

Shafike, N.G., S.A. Bawazir, and J. Cleverly, 2007. Native Versus Invasive Plant Water Use in the Middle Rio Grande Basin. Southwest Hydrology 6:28-29.

Šimunek, J., M. Šejna, H. Saito, M. Sakai, and M.T.v. Genuchten, 2008. The HYDRUS-1D Software Package for Simulating the Movement of Water, Heat, and Multiple Solutes in Variably Saturated Media, Version 4.0, HYDRUS Software Series 3, Department of Environmental Sciences, University of California Riverside, Riverside, California, 315 pp.

Smith, E.A., A.Y. Hsu, W.L. Crosson, R.T. Field, L.J. Fritschen, R.J. Gurney, E.T. Kanemasu, W.P. Kustas, D. Nie, W.J. Shuttleworth, and others, 1992. Area-Averaged Surface Fluxes and Their Time-Space Variability over the FIFE Experimental Domain. Journal of Geophysical Research 97(D17): 18599-18622.

Soil Science Glossary Terms Committee, 2008. Glossary of Soil Science Terms 2008. Soil Science Society of America, Madison, Wisconsin, 92 pp.

Soil Survey Staff, 2013. Soil Survey Geographic (SSURGO) Database for (Angeles National Forest, California). http://soildatamart.nrcs.usda.gov, *accessed* January 2013.

S.S. Papadopulos & Associates, Inc., 2006. Riparian Groundwater Models for the Middle Rio Grande: ESA Collaborative Program FY04. Report prepared for the New Mexico Interstate Stream Commission, 69 pp.

Stein, E., A. Guber, and A. Dembovetsky, 2004. Key Soil Water Contents. *In*: Development of Pedotransfer Functions in Soil Hydrology, Y. Pachepsky and W.J. Rawls (Editors). Elsevier, Amsterdam, pp. 241-249.

Toll, D., 2008. Benchmark Report for the EPA BASINS Decision Support Tool. Report, Hydrological Sciences Branch, NASA Goddard Space Flight Center, Greenbelt, Maryland, 52 pp.

Trezza, R., R. Allen, and M. Tasumi, 2013. Estimation of Actual Evapotranspiration along The Middle Rio Grande of New Mexico Using MODIS and Landsat Imagery with the METRIC Model. Remote Sensing 5(10):5397.

U.S. Bureau of Reclamation, 1997. Middle Rio Grande Water Assessment: Middle Rio Grande Land Use Trend Analysis Geographic Information System Data Base. U.S. Bureau of Reclamation, Albuquerque Area Office, Albuquerque, New Mexico.

U.S. Geological Survey, 2008. Documentation of Computer Program INFIL3.0-A Distributed-Parameter Watershed Model to Estimate Net Infiltration below the Root Zone, USGS Scientific Investigations Report 2008-5006, 98 pp.

Vachaud, G., A. Passerat De Silans, P. Balabanis, and M. Vauclin, 1985. Temporal Stability of Spatially Measured Soil Water Probability Density Function. Soil Science Society of America Journal 49(4):822-828.

Van Hylckama, T.E.A., 1974. Water Use by Salt Cedar as Measured by the Water Budget Method. U.S. Geological Survey Professional Paper 491-E, 30 pp.

Vereecken, H., J.A. Huisman, H. Bogena, J. Vanderborght, J.A. Vrugt, and J.W. Hopmans, 2008. On the Value of Soil Moisture Measurements in Vadose Zone Hydrology: A Review. Water Resources Research 44: W00D06.

Wagenet, R.J. and J.L. Hutson, 1996. Scale-Dependency of Solute Transport Modeling/GIS Applications. Journal of Environmental Quality 25:499-510.

Western States Water Council, 2012. The Landsat Program and Water Resources Information Needs in the United States. http://www.kimberly.uidaho.edu/water/metric/Essential_Specifications_for_Landsat-WSWC_Apr_9_12.pdf, *accessed* January 2013.

White, W.N., 1932. A Method of Estimating Groundwater Supplies Based on Discharge by Plants and Evaporation from Soil. USGS Water Supply Paper 654A, Washington, D.C., 106 pp.

Winsemius, H.C., H.H.G. Savenije, and W.G.M. Bastiaanssen, 2008. Constraining Model Parameters on Remotely Sensed Evaporation: Justification for Distribution in Ungauged Basins? Hydrology and Earth System Sciences 5:2293-2318.

Wohl, E., A. Barros, N. Brunsell, N.A. Chappell, M. Coe, T. Giambelluca, S. Goldsmith, R. Harmon, J.M.H. Hendrickx, J. Juvik, J. McDonnell, and F. Ogden, 2012. The Hydrology of the Humid Tropics. Nature Climate Change 2:655-662, DOI: 10.1038/nclimate1556.